NAVAL POSTGRADUATE SCHOOL

MONTEREY, CALIFORNIA

THESIS

THE EXTRATROPICAL TRANSITION OF TROPICAL STORM BANYAN

by

Michael D. Vancas

September 2006

Thesis Advisor:	Patrick Harr
Second Reader:	Russell Elsberry

THIS PAGE INTENTIONALLY LEFT BLANK

REPORT DOCUMENTATION PAGE			*Form Approved OMB No. 0704-0188*
Public reporting burden for this collection of information is estimated to average 1 hour per response, including the time for reviewing instruction, searching existing data sources, gathering and maintaining the data needed, and completing and reviewing the collection of information. Send comments regarding this burden estimate or any other aspect of this collection of information, including suggestions for reducing this burden, to Washington headquarters Services, Directorate for Information Operations and Reports, 1215 Jefferson Davis Highway, Suite 1204, Arlington, VA 22202-4302, and to the Office of Management and Budget, Paperwork Reduction Project (0704-0188) Washington DC 20503.			
1. AGENCY USE ONLY ***(Leave blank)***	**2. REPORT DATE** September 2006	**3. REPORT TYPE AND DATES COVERED** Master's Thesis	
4. TITLE AND SUBTITLE The Extratropical Transition of Tropical Storm Banyan			**5. FUNDING NUMBERS**
6. AUTHOR Michael Vancas			
7. PERFORMING ORGANIZATION NAME(S) AND ADDRESS(ES) Naval Postgraduate School Monterey, CA 93943-5000			**8. PERFORMING ORGANIZATION REPORT NUMBER**
9. SPONSORING /MONITORING AGENCY NAME(S) AND ADDRESS(ES) N/A			**10. SPONSORING/MONITORING AGENCY REPORT NUMBER**
11. SUPPLEMENTARY NOTES The views expressed in this thesis are those of the author and do not reflect the official policy or position of the Department of Defense or the U.S. Government.			
12a. DISTRIBUTION / AVAILABILITY STATEMENT Approved for public release; Distribution is unlimited			**12b. DISTRIBUTION CODE**
13. ABSTRACT During July 2005, Typhoon Banyan recurved and underwent extratropical transition over the western North Pacific. Coincident with the extratropical transition of Banyan, a large mid-tropospheric anticyclone developed immediately east of the recurving typhoon. The anticyclone was associated with a high-amplitude, Rossby wave-like pattern that developed downstream of the anticyclone and extended across the North Pacific. Development of the anticyclone is examined with respect to the interaction between the outflow from Banyan and the midlatitude jet streak. During the poleward movement of TY Banyan, an anticyclonically-curved jet streak was forced by the merger of the upper-level outflow from Banyan and a jet streak associated with an upstream trough. The anticyclonic curvature was accentuated by the presence of a mid-tropospheric cyclone east of Banyan. The anticyclonic curvature increased as Banyan moved poleward and the mid-tropospheric cyclone moved equatorward. Thermodynamic forcing of the mid-tropospheric anticyclone is examined with respect to the poleward movement of warm moist air that ascends as it is advected around the eastern side of the decaying typhoon. The combination of dynamic and thermodynamic factors is examined in a potential vorticity framework to identify the development of the anticyclone east of Banyan and the transformation of Banyan into a midlatitude cyclone.			
14. SUBJECT TERMS Tropical Cyclones, Extratropical Transition, Banyan, Advanced Microwave Sounding Unit, Potential Vorticity, Polar-orbiting Satellites			**15. NUMBER OF PAGES** 90
			16. PRICE CODE
17. SECURITY CLASSIFICATION OF REPORT Unclassified	**18. SECURITY CLASSIFICATION OF THIS PAGE** Unclassified	**19. SECURITY CLASSIFICATION OF ABSTRACT** Unclassified	**20. LIMITATION OF ABSTRACT** UL

THIS PAGE INTENTIONALLY LEFT BLANK

Approved for public release; distribution is unlimited

THE EXTRATROPICAL TRANSITION OF TROPICAL STORM BANYAN

Michael D. Vancas
Lieutenant, United States Navy
B.S., Texas A & M, 1999

Submitted in partial fulfillment of the
requirements for the degree of

**MASTER OF SCIENCE IN
METEOROLOGY AND PHYSICAL OCEANOGRAPHY**

from the

**NAVAL POSTGRADUATE SCHOOL
September 2006**

Author: Michael David Vancas

Approved by: Patrick Harr
Thesis Advisor

Russell Elsberry
Second Reader

Phil Durkee
Chairman, Department of Meteorology

THIS PAGE INTENTIONALLY LEFT BLANK

ABSTRACT

During July 2005, Typhoon Banyan recurved and underwent extratropical transition over the western North Pacific. Coincident with the extratropical transition of Banyan, a large mid-tropospheric anticyclone developed immediately east of the recurving typhoon. The anticyclone was associated with a high-amplitude, Rossby wave-like pattern that developed downstream of the anticyclone and extended across the North Pacific. Development of the anticyclone is examined with respect to the interaction between the outflow from Banyan and the midlatitude jet streak. During the poleward movement of TY Banyan, an anticyclonically-curved jet streak was forced by the merger of the upper-level outflow from Banyan and a jet streak associated with an upstream trough. The anticyclonic curvature was accentuated by the presence of a mid-tropospheric cyclone east of Banyan. The anticyclonic curvature increased as Banyan moved poleward and the mid-tropospheric cyclone moved equatorward. Thermodynamic forcing of the mid-tropospheric anticyclone is examined with respect to the poleward movement of warm moist air that ascends as it is advected around the eastern side of the decaying typhoon. The combination of dynamic and thermodynamic factors is examined in a potential vorticity framework to identify the development of the anticyclone east of Banyan and the transformation of Banyan into a midlatitude cyclone.

THIS PAGE INTENTIONALLY LEFT BLANK

TABLE OF CONTENTS

THIS PAGE INTENTIONALLY LEFT BLANK

LIST OF FIGURES

THIS PAGE INTENTIONALLY LEFT BLANK

LIST OF ABBREVIATIONS

AMSU	Advanced Microwave Sounding Unit
ET	Extratropical Transition
IR	Infra-Red
TC	Tropical Cyclone
WV	Water-Vapor
CIRA	Cooperative Institute for Research in the Atmosphere
NCEP	National Centers for Environmental Prediction
NOGAPS	Navy Operational Global Atmopheric Prediction System
GFS	Global Forecast System
K	Degrees Kelvin
kt	Nautical Miles per hour
M	Meter
S	Second
GrADS	Grid Analysis and Display System
CLW	Cloud Liquid Water
PW	Precipitable Water
T	Temperature
P	Pressure
TD	Tropical Depression
LAT	Latitude
LON	Longitude
ASCII	American Standard Code for Information Interchange
hPa	hecto-Pascals
STS	Severe Tropical Storm
PVA	Potential Vorticity Anomaly

THIS PAGE INTENTIONALLY LEFT BLANK

ACKNOWLEDGMENTS

I would like to thank my friends and family for understanding and supporting me during the writing process. I could not have completed this work without their unconditional support.

The incredibly patient teaching, re-teaching, coding, reading, editing, re-editing and re-re-editing conducted by my advisors Professor Harr and Professor Elsberry was invaluable. Thank you both so much for your patience and expertise!

Dr. John Knaff of CIRA provided invaluable assistance generating the AMSU data for this study.

Jeff Hawkins and the Navy Research Laboratory-Monterey satellite team provide polar-orbiting satellite data.

THIS PAGE INTENTIONALLY LEFT BLANK

I. INTRODUCTION

Every year, tropical cyclones (TCs) develop in the low-latitude regions of the ocean basins of the world. After following a generally northwestward (Northern Hemisphere) track, many TCs move to higher latitudes during their life cycle. This track takes the TC away from its energy source into a region of lower sea-surface temperatures, and increased baroclinicity and vertical wind shear. Upon encountering lower sea-surface temperatures, increased vertical wind shear and/or achieving landfall, the TC undergoes a period of weakening and eventually dissipates. However, many of the Atlantic and western North Pacific TCs that cross 30° N interact with the baroclinic environment of the midlatitudes in a manner that leads to the transformation from a tropical cyclone to an extratropical cyclone (Evans and Hart 2003). This period in the life cycle of the TC is called the extratropical transition.

A. DEFINING EXTRATROPICAL TRANSITION

Although there have been many attempts to characterize the stages of the ET, no commonly accepted definition of ET exists. Matano and Sekioka (1971) identified two characteristic types of ET in the western North Pacific. The first is a “complex transition,” which occurs through the interaction of a TC and a pre-existing midlatitude front or trough. The second characteristic type is a “compound” transition, which involves the interaction of the TC and a midlatitude cyclone. Brand and Guard (1979)

identified a third type of ET that occurs during the dissipation of the TC as it moves into the midlatitude environment.

During the period 1990-1997, at least one ET event occurred over the western North Pacific during all months except February (Harr and Elsberry 2000). On average, Southern Hemisphere ET is completed by 30° S (Sinclair 2002), but storms in the Northern Hemisphere can preserve tropical characteristics as far north as 50°N (Jones et al. 2003). Forty-five percent of Atlantic storms (more than any other basin) undergo ET, with over 60% of these storms maintaining intensity or strengthening (Evans and Hart 2003).

Klein et al. (2000) studied cases of ET in the western North Pacific occurring during July-October 1994-96 and proposed that an ET has two stages. In the cases studied by Klein et al., the transformation stage from a symmetric warm-core TC system to a baroclinic, extratropical system occurred in the same sequential fashion. They noted that not all TCs undergoing ET successfully underwent re-intensification as an extratropical cyclone, and thus dissipated rather than completing an ET.

Several factors control the re-intensification or dissipation of a transitioning TC. The physical mechanisms found to favor extratropical re-intensification include the approach of an upper-level midlatitude trough from the west, the presence of a lower-tropospheric horizontal temperature gradient, and the distribution of water vapor. Factors contributing to the dissipation of landfalling TCs include the increased surface drag, reduction of surface

fluxes of latent and sensible heat, and orographic disruptions to the flow (Jones et al., 2003).

Two characteristic midlatitude circulation patterns were identified in a study by Harr and Elsberry (2000) of 30 ET cases in the western North Pacific. The first is the Northwest pattern, which is defined such that the ET occurs downstream of a midlatitude trough with the midtropospheric potential vorticity maximum to the northwest of the decaying TC. The second case is the Northeast pattern in which the dominant midlatitude circulation is a quasi-stationary cyclone to the northeast of the TC center. These two patterns result in different tracks and re-intensifications of the extratropical cyclone in the ET. During June to October 1994-1997, 30 storms (of 112 total) completed ET in the western North Pacific (Klein et al. 2000). It was noted that 13 of the 30 cases translated into a Northeast pattern and 17 into a Northwest pattern as defined by Harr and Elsberry (2000), with the Northwest cases resulting in significantly lower sea-level pressures than the Northeast cases.

Generally, ET is considered a gradual process that is initiated by environmental changes occurring as the TC moves poleward and the TC loses tropical characteristics and becomes extratropical in nature. Because the TC often undergoes re-intensification and/or acceleration during the ET process, categorization and understanding of the key parameters initiating and controlling ET are critical to the early identification and prediction of TCs that will most likely experience a transition.

B. OBSERVING AND FORECASTING CHALLENGES

The extratropical transition (ET) of a tropical cyclone affects the track direction and translation speed, intensity, circulation size, precipitation and landfall probability. Cyclones undergoing ET often become fast-moving and explosively-developing extratropical cyclones (Jones et al. 2003). The potential for these storms to produce gale-force winds and heavy precipitation makes these events exceedingly important to civil and military agencies. Additionally, recent studies have highlighted the influence of ET events on synoptic-scale circulations far downstream of the tropical cyclone location.

It is well known that extratropical cyclones will bring high winds and heavy precipitation to coastal regions during the winter in the midlatitudes. Due to the seasonal nature of many recreational activities along the coasts, coastal populations are at a maximum during the warm summer and early fall months, which are coincident with the peak hurricane/typhoon season. It is less well known that extratropical transition of a TC can bring hurricane-like conditions to unprepared midlatitude coastal regions that may result in flooding, billions of dollars in damage, and loss of life. Accurate forecasts of the intensity and movement of TCs undergoing ET are thus absolutely critical to warn the public of these potentially hazardous conditions.

Tropical cyclone forecasts are highly dependent on the accuracy of the current TC structure, intensity, and position. Observing the large variations in atmospheric parameters associated with TCs is the first challenge in

the forecasting process. Tropical cyclones develop over data-sparse regions, which limits the accuracy of the TC model initialization. Since the introduction of remotely-sensed data, observational capabilities with regard to TCs over the ocean basins have vastly improved. Infrared (IR) and visible imagery provides critical information on the atmospheric thermodynamic parameters and dynamics associated with TCs. A key observational tool for ET is the water-vapor imagery that identifies TC outflow into the midlatitudes. However, infrared, visible, and water-vapor imagery cannot resolve the multi-level atmospheric gradients in the cloudy regions, which limits the utility of these techniques. Microwave soundings from polar-orbiting satellites do allow examination of the parameters and gradients of the TC and its environment in the cloudy regions, with the exception of regions of heavy precipitation or where uncertainty in the emissivity of the underlying land surface may limit the accuracy of the microwave soundings.

C. OBJECTIVE OF THE THESIS

The primary objective of this study is to further examine the benefits of microwave imagery in observing the conditions leading to the ET process in the western North Pacific. As stated above, the re-intensification process depends on various environmental factors. Many of these factors involve gradients of atmospheric variables not easily observed with current “in situ” observational systems due to the limited availability of observation sites in oceanic regions. Furthermore, the forcing of downstream impacts may be dependent on specific dynamic and

thermodynamic processes that are difficult to diagnose in conventional numerical analyses. Therefore, remotely sensed data of important environmental conditions are essential to observe important variables that would aid in the prediction of subsequent ET characteristics. This thesis will explore the usefulness of the Advanced Microwave Sounding Unit (AMSU) for observing the thermal structure.

The organization of the thesis is the following. In Chapter II, a brief overview of the AMSU is presented, and this is followed by discussion of the data processing used in the thesis. In Chapter III, a discussion of the case study used in the thesis is presented. Finally, the summary of results, conclusions, and recommendations for future research are contained in Chapter IV.

II. DATA

Microwave sounding instruments have been placed on numerous earth-observing systems in recent years. Microwaves have very long wavelengths, and thus pass easily through obscuring clouds, although exhibiting sensitivity to precipitation-sized droplets. Depending on the wavelength, two primary atmospheric constituents affect microwave transmittance: oxygen and water vapor. Because of this sensitivity, microwave imagery provides information on two atmospheric variables important to the ET process: temperature (through oxygen emissions) and water vapor concentration. The Advanced Microwave Sounding Unit (AMSU) is one of the recently deployed microwave satellite instruments and is used extensively in this study.

A. SATELLITE DATA AND PROCESSING

1. AMSU-A Instrument

The AMSU-A is a cross-track, line-scanning instrument that scans the earth over 30 angles for 6 seconds, then scans cold space and the satellite body (as a black-body calibration target) for one second each. This scan geometry results in a 2393 km swath width from an orbit altitude of 833 km with a maximum horizontal resolution of 40 km at nadir.

The AMSU-A instrument measures outgoing microwave radiance in 15 channels and its primary function is to estimate atmospheric temperature profiles from the surface to 40 km elevation. However, atmospheric water vapor and precipitation rate estimates are provided as well. The

instrument is divided into two modules called A1 and A2. The A1 module contains channels 3-15 that measure radiances between 50.3 and 57.29 GHz (channels 3-14) and at 89.0 GHz (channel 15). Module A2 senses radiances for channels 1 and 2 at 23.8 and 31.4 GHz, respectively (see Figure 1).

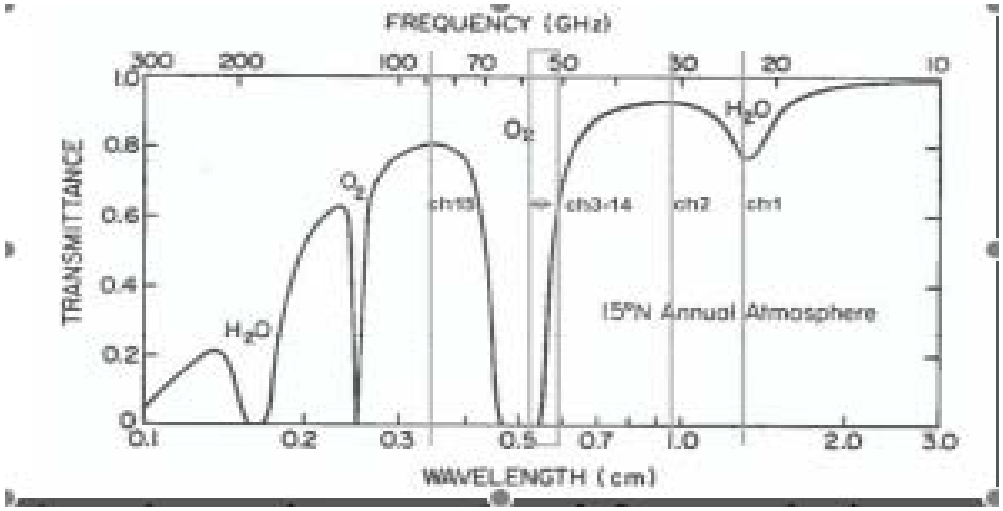

Figure 1. The AMSU-A channel frequency bands (vertical lines) as compared to the standard atmospheric water vapor and oxygen windows (curved solid lines) (after Stubblefield 2005).

Channel 1 is at the center of a water vapor absorption band, which makes channel 1 very sensitive to atmospheric water vapor concentration. Since channel 2 falls in a relative absorption window, it is sensitive to ocean surface wind speed and precipitation. Channels 3-14 fall within a strong oxygen absorption band. Channels 3 and 4 are near the edge of the absorption band, and retrieve radiance values from the surface and lower atmosphere. The remaining channels (5 - 14) are closer to the center of the absorption band, and retrieve radiances from progressively higher in the atmosphere, as illustrated in the weighting

function diagram (Figure 2). Channel 15 senses another relative absorption window, although at a higher frequency (shorter wavelength) and is sensitive to cloud properties including precipitation. Channel 7 is used here to study the upper tropospheric TC structures due to the elevation of the weighting function peak.

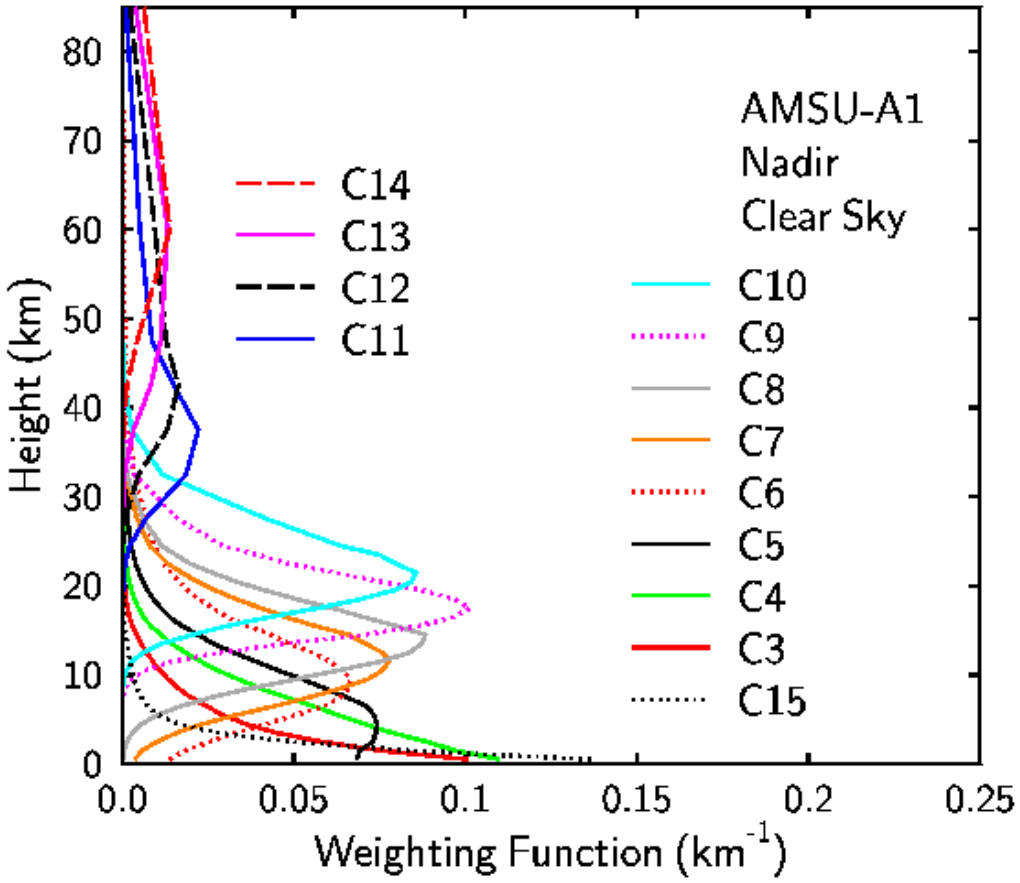

Figure 2. The AMSU-A channel 3-15 weighting functions from the Cooperative Institute for Research in the Atmosphere website http://amsu.cira.colostate.edu/.

2. AMSU-B Instrument

The AMSU-B is the channels 16-20 of the AMSU instrument package. This five-channel microwave radiometer is designed to measure atmospheric humidity from a number

of different atmospheric layers. Similar to AMSU-A, the AMSU-B instrument is a cross-track, line-scanning passive microwave radiometer. The antenna rotates with a period of 2.67 seconds in a plane perpendicular to the instrument, with a constant beamwidth of 1.1 degrees. The sampling method of this instrument allows a maximum horizontal resolution of 16 km at nadir at a nominal 850 km elevation. Channels 16 and 17 of the AMSU-B instrument are in a relative absorption window, and thus retrieve radiances from near the earth surface (see Figure 3). Channels 18 - 20 retrieve radiances in the 183 GHz water vapor absorption band.

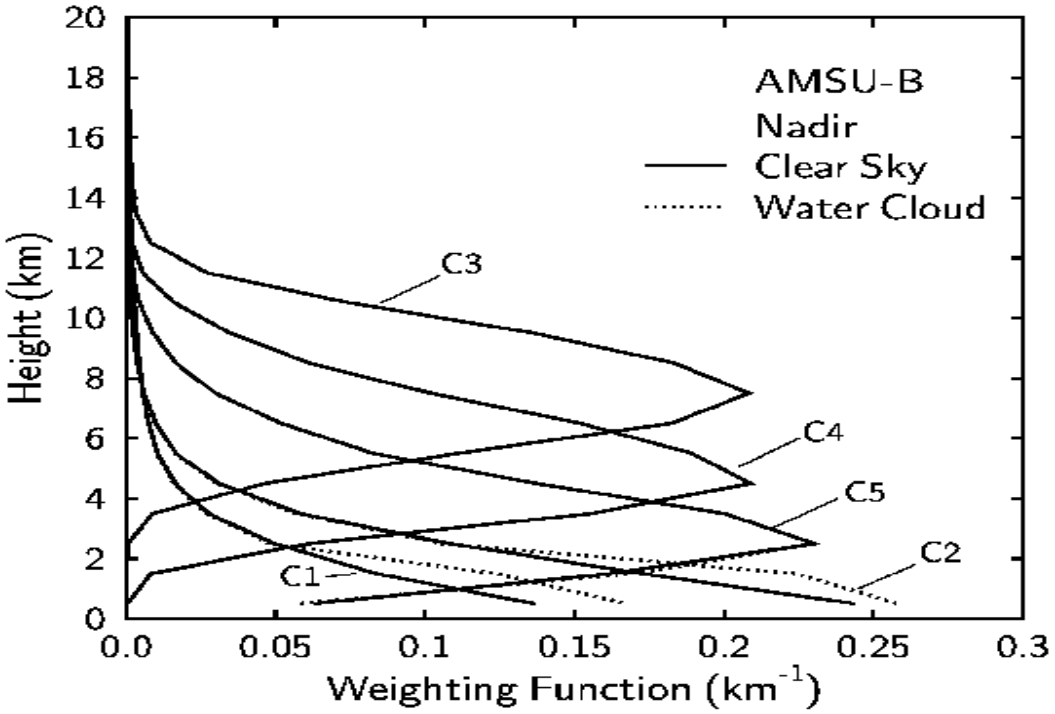

Figure 3. The AMSU-B weighting functions with C1, C2, C3, C4, and C5 corresponding to AMSU-B channels 16, 17, 18, 19, and 20 in the text, respectively. The dashed lines are the weighting function in the presence of a water cloud between 950 hPa and 750 hPa. (from the CIRA website http://amsu.cira.colostate.edu/).

3. Satellite Processing

The AMSU data are processed in several steps. The two primary corrections are the limb correction and the antenna correction. The limb correction accounts for the increased optical path length for scan angles that are off nadir. The antenna correction accounts for contributions to the received radiance values due to antenna side lobes.

Limb correction approaches have been developed using statistical, physical, or a combination of statistical and physical methods (Goldberg et al., 2001). A purely physical approach has been found to be impractical due to the asymmetries in the nadir weighting functions (Goldberg et al., 2001) that are shown in Figures 2 and 3. Limb corrections in this study were based on a statistical algorithm provided by the Cooperative Institute for Meteorological Satellite Studies.

The second primary correction that must be made is the antenna correction, which converts the raw radiance values into brightness temperatures. Radiance measurements are made between 48° off nadir at 30 scan angles or positions. The majority of the radiance retrieved by the antenna (~95%) is from the main lobe, and the remainder (~5%) is due to side lobes (Mo 1999). It is because the side lobes receive contributions from the satellite body and space that an antenna adjustment is required. Mo (1999) developed equation (2.1) to convert the raw antenna temperature T_A to brightness temperature T_E:

$$T_A(\beta) = \frac{1}{N_\eta}\left[f_e(\beta)\overline{T_E} + f_c(\beta)\overline{T_C} + f_{sat}(\beta)\overline{T_{SAT}}\right] \quad (2.1)$$

$$N_\eta = f_e + f_c + \eta f_{sat} \quad (2.2)$$

where T_C is the temperature of cold space, T_{Sat} is the temperature of the satellite, f_e, f_C, and f_{Sat} are the antenna frequencies of the earth, cold space, and the satellite, respectively, η is a channel specific scale factor and β is the scan angle. In calculating T_E above, it is assumed that T_C is a constant 2.73 K, and that T_{Sat} is negligible because its maximum contribution is on the order of 0.001 K.

B. TEMPERATURE, WIND, AND PRESSURE FIELD RETRIEVALS

The methods discussed in Chapter II.A. result in brightness temperature fields for each channel. Although these brightness temperatures provide useful data, further processing is required for this research. Weng and Yan (2000) developed an algorithm to generate land-surface temperatures (Eq. 2.3), which are required to display brightness temperature data in a more useful format,

$$T_S = 37.700 + 0.38057TB_1 - 0.39747TB_2 + 0.94279TB_3 . \qquad (2.3)$$

Temperature (and winds to be described below) fields at all levels were then generated using an algorithm provided by Dr. John Knaff of the Cooperative Institute for Research in the Atmosphere (CIRA) and first developed by Demuth et al. (2004). After applying the antenna and limb corrections discussed above to generate brightness temperatures for all channels, the radiances are used in a statistical method (Goldberg et al. 2000, Knaff et al. 2000) to generate temperature as a function of pressure at 40 levels ranging from 1000 to 0.1 hPa (Demuth et al. 2004). The algorithm is applied at 23 pressure levels between 920 and 50 hPa, and assumes that the 1000 hPa level

is below the surface in strong TCs and that the 50 hPa level is above the storm circulation.

The attenuation of microwave radiation in the presence of large hydrometeor particles results in abnormally low brightness temperatures, which affects the retrieved temperatures, derived pressure fields, and other derived products. To counter this effect, Demuth et al. (2004) developed one correction for the attenuation caused by cloud liquid water (CLW) and a second correction for the scattering caused by ice crystals. The algorithm used in this study includes both of these corrections.

The temperature profiles were first corrected using the CLW correction at the AMSU-A swath points. The two-pass distance-weighted analysis method developed by Barnes (1964) was used to interpolate the temperature and CLW data on the swath to a 12˚ lat. × 12˚ lon. grid with a 0.2˚ lat. grid interval. The second hydrometeor correction is then applied to correct the interpolated data for ice scattering (Demuth et al., 2004).

The Barnes analysis technique results in some smoothing of the data that depends on the value of the *e*-folding radius selected. Demuth et al. (2004) chose an *e*-folding radius based upon the behavior of the response function for a range of radii between 50-150 km. They subjectively determined that the minimum value that sufficiently smoothed the retrieved fields (based on contour plots) was 100 km. Thus, this value is used in the Barnes analysis for this study.

To retrieve horizontal wind fields, Demuth et al. (2004) assume hydrostatic and gradient wind balance. Their

algorithm interpolates the hydrometeor-corrected temperatures to a cylindrical grid with the TC center at the origin. Since surface temperature cannot be derived from AMSU data, the National Centers for Environmental Prediction (NCEP) global analysis surface temperature at the time closest to the AMSU swath time was used. The Demuth et al. algorithm only uses the NCEP surface temperature as a lower boundary condition to derive the surface pressure (Demuth et al., 2004). The primary contribution to the surface pressure gradient will come from the temperature structure above the surface via the downward integration of the hydrostatic equation.

The next step in deriving the wind field is the calculation of the geopotential height field as a function of pressure via the hydrostatic equation. Further assumptions must be made: i) temperature varies linearly with height between two pressure levels; ii) variations in gravity with height are negligible; and iii) virtual temperature effects can be neglected. Demuth et al. (2004) noted that the third assumption can lead to errors of a few hectopascals in the surface pressure, and that those potential errors are proportional to the moisture gradient vice the total moisture field.

The Demuth et al. (2004) algorithm begins with the integration of the hydrostatic equation at the outer-most radius of the domain, where the surface pressure boundary condition was determined from the same NCEP analysis used for the surface temperature. The hydrostatic equation was integrated upward to 50 hPa to give the heights at the AMSU pressure levels at a radius r = 600 km. The height of the

50 hPa surface was then assumed to be constant, since it is above all perturbations caused by the TC at all radii. The hydrostatic equation is then integrated downward from 50 hPa to 920 hPa at all radii in the interior of the domain. Based on the height and temperature of the 920 hPa level and the surface temperature from the NCEP analysis, the hydrostatic equation was integrated downward (from 920 hPa to the surface) to compute the surface pressure at all points in the domain. With the assumption of a linear variation in temperature with height between AMSU levels, the temperatures and pressures were determined at 1-km vertical intervals to 20 km. Finally, the density at each level was calculated using the ideal gas equation (Demuth et al., 2004).

Once temperature, pressure, and density are known as functions of height and radius, the tangential wind field can be determined assuming gradient wind balance:

$$\frac{V^2}{r} + fV = \frac{1}{\rho}\frac{\partial p}{\partial r} \qquad (2.4)$$

where p is the pressure, ρ is the density (both known functions), r is the radius, f is the Coriolis parameter (evaluated at the storm center), and V is the magnitude of the wind speed.

The algorithm supplied by Dr. Knaff generates ASCII text files containing tabulated listings of the latitude, longitude, winds (u and v components), temperature, and height. The text files also contain the surface pressure and CLW information. These text files are used to generate the various plan views, graphs, and charts for this study.

C. NUMERICAL MODEL FIELDS

This case study utilizes a combination of numerical model fields, visible, infrared (IR), water vapor (WV), and microwave satellite imagery, and derived products to analyze the extratropical transition of TC Banyan during 25-28 July 2005.

1. NOGAPS Fields

The Navy Operational Global Atmospheric Prediction System (NOGAPS) model fields and ensemble products provided by Naval Research Laboratory-Monterey are used in this study. The NOGAPS 0000 UTC and 1200 UTC analyses were used to examine TC structure and dynamics as compared to IR, WV, and when available, microwave imagery. Because the 0600 UTC and 1800 UTC analyses were not available, the 6-h forecasts from the 0000 UTC and 1200 UTC model integrations, respectively were substituted to provide a 6-hour time resolution. Analyses of 500 hPa heights, 200 hPa winds, 500 hPa omega, potential temperature, and model-generated soundings were used to compute various diagnostics and to identify features that aided or inhibited the TC throughout the ET period.

2. GFS Fields

The NCEP Global Forecast System (GFS) model fields were used in conjunction with the NOGAPS fields discussed above. The GFS 0000 UTC and 1200 UTC analyses were used to examine the TC structure, and the 6-h forecasts from the 0000 UTC and 1200 UTC model integrations were used to provide a 6-hour time resolution. Analyses of 500 hPa heights, 200 hPa winds, 500 hPa omega, potential temperature, and model-generated soundings were used to compute various diagnostics and to identify features that

aided or inhibited the TC throughout the ET period. Global Forecast System model fields were also compared to IR and WV imagery, and when available, to microwave data to complete the analysis of the ET processes for this case.

3. Ensemble Products

Naval Research Laboratory—Monterey provided ensemble products based on the NOGAPS model. The ensemble products were used to examine the effect of model uncertainty on the ET process. Jones et al. (2003) state: “The relatively small scale of the tropical cyclone and the complex physical processes that occur during the interactions between a tropical cyclone and the midlatitude environment present difficult numerical forecast problems.” The degradation of model forecast skill as a result of an ET event can extend across an entire ocean basin. This study will examine some of the effects of the ET process on ensemble spread and uncertainty.

THIS PAGE INTENTIONALLY LEFT BLANK

III. TYPHOON BANYAN: A CASE STUDY

Typhoon Banyan (07W) was a western North Pacific typhoon that successfully completed the ET process during July 2005. This study applies the principles and techniques discussed in Chapter II to identify critical structural and environmental changes in TY Banyan during the ET process. Furthermore, the impact of the ET of Banyan on the synoptic-scale circulation of the western North Pacific is examined.

The extratropical transition of TY Banyan coincided with the formation of a large tropospheric anticyclone (Figure 4) that covered much of the western North Pacific basin north of 40°N. This ridge, along with the decaying tropical cyclone that reintensified as an extratropical cyclone, formed part of an extensive wave train that stretched across the Pacific basin from Asia to the North American continent (Figure 4). Typhoon Banyan is represented by a large area of anomalous low heights over Japan, while the large ridge dominating the western North Pacific is downstream of Banyan.

The extratropical transition of a tropical cyclone introduces a large amount of uncertainty into atmospheric prediction models, which is represented by an increase in standard deviation in the 500 hPa height in the ensemble members (Figure 5). The large plume of increased standard deviation between ensemble members in the GFS prediction system introduced by the ET of TY Banyan and the downstream ridge begins 36 h into the integration initialized 1200 UTC 26 July.

Several studies (Klein et al. 2000, Hart and Evans 2000, Harr and Elsberry 2000, and others) have focused primarily on the low-pressure system that results from an ET event. This study will also focus on the dynamics associated with the building ridge downstream of the transforming TC. This process is important to the resulting synoptic environment of the western North Pacific and merits detailed examination as it may be a major source of the variability defined in Figure 5.

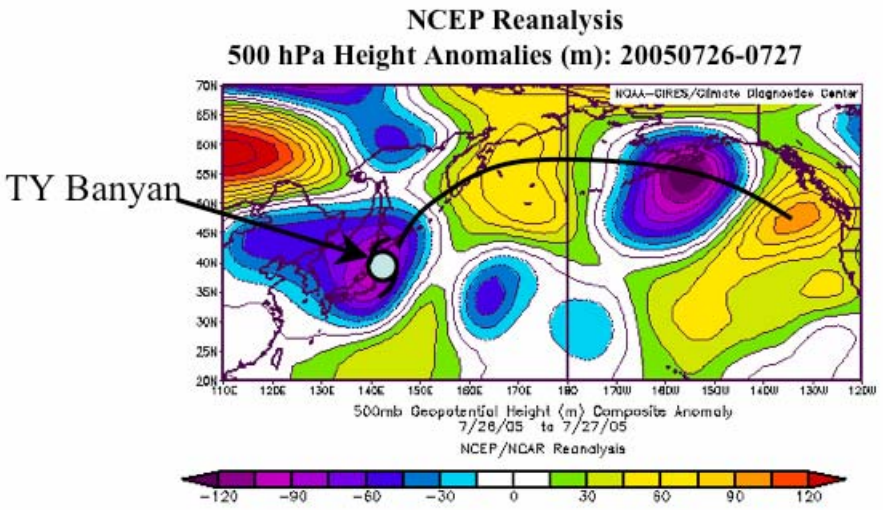

Figure 4. Height anomalies at 500 hPa produced by the NCEP/NCAR system for 26 July - 27 July 2005. The hurricane symbol marks the 0000 UTC 26 July position of TY Banyan and the arc associated with the Rossby wave train is defined by the solid black line.

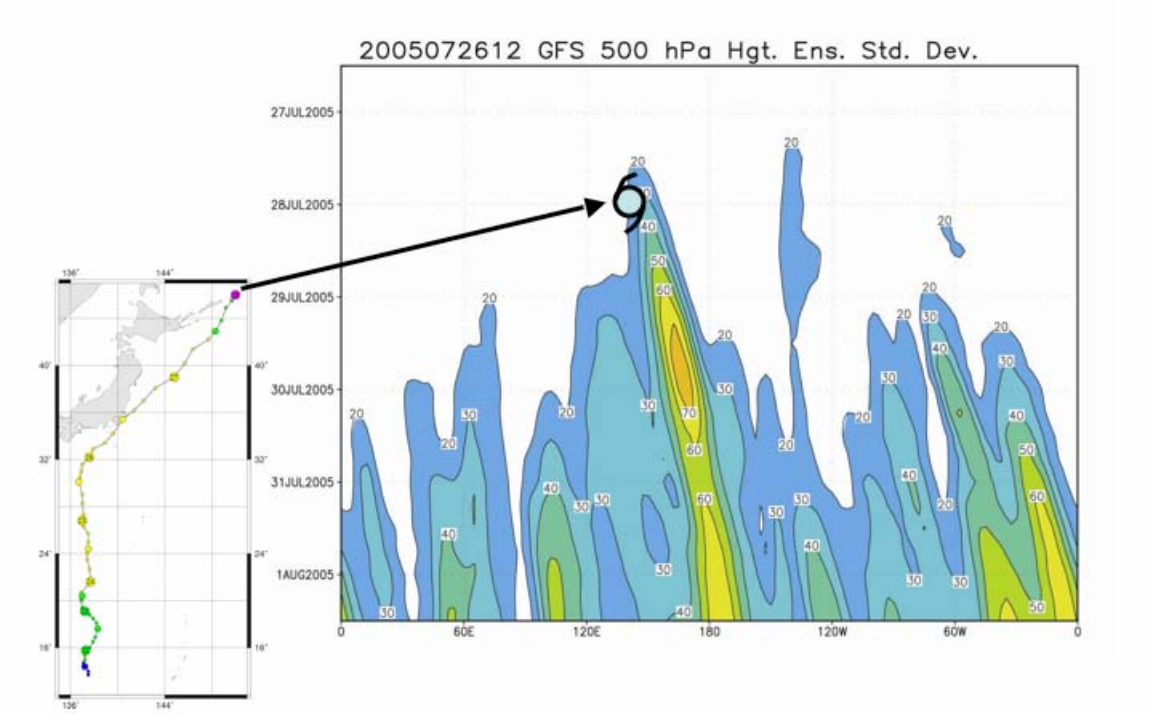

Figure 5. Time-longitude plot of 500 hPa height standard deviation (m) of the ensemble members from the GFS ensemble prediction system.

A. TYPHOON BANYAN TRACK AND SYNOPTIC OVERVIEW

Typhoon Banyan (Figure 6) was classified as a tropical depression (TD) at 1800 UTC 21 July 2005 at 15.1˚N, 137.3˚E. Banyan then moved northward and strengthened over the next 48 hours to achieve a minimum central pressure of 975 hPa (Figure 7) with sustained winds of 55 kt. Banyan continued on a northward track until late on 25 July, when the storm weakened slightly and turned to the northeast. This generally northeastward track continued until the storm was classified as being extratropical at 0000 UTC 28 July and began to follow a more zonal track (Figure 6).

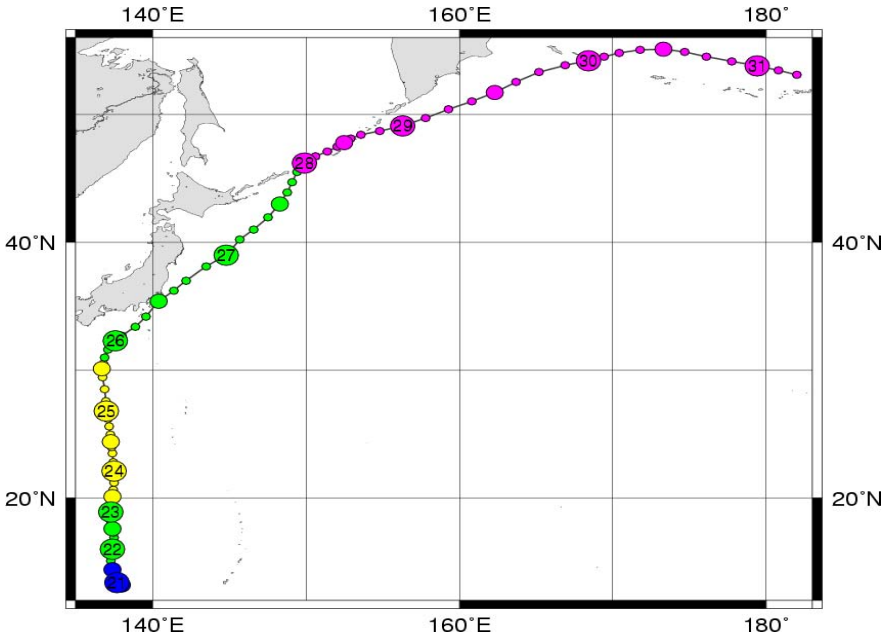

Figure 6. Track of TY Banyan (07W) in 3-h increments with color-coding defined as: blue indicates tropical depression (international class 2), green indicates tropical storm (int'l. class 3, JMA Typhoon), yellow indicates severe tropical storm (int'l. class 4) and magenta indicates an extratropical cyclone (int'l. class 6) (from: http://agora.ex.nii.ac.jp/digital-typhoon/summary/wnp/1/200507.html.en).

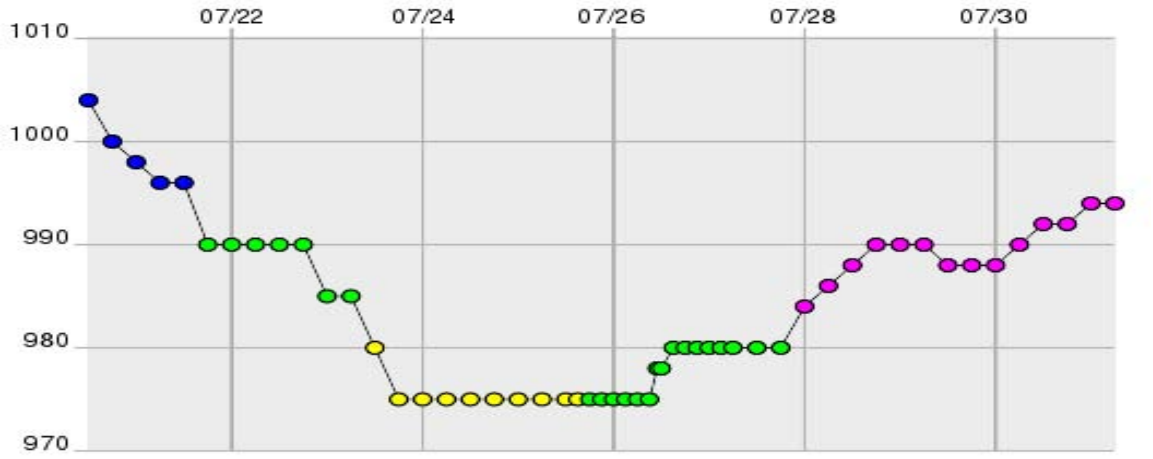

Figure 7. Central pressure of TY Banyan (07W) versus date with color-coding as described in Figure 6 (source: http://agora.ex.nii.ac.jp/digital-typhoon/summary/wnp/1/200507.html.en).

1. Large-scale Midtropospheric Environment of Banyan

As TY Banyan approached southern Japan at 0000 UTC 25 July, the western North Pacific basin was dominated by the subtropical ridge and a series of midtropospheric cyclonic cells propagating eastward from the coast of Asia (Figure 8). These circulations eventually weakened the subtropical ridge enough to allow the northward movement of TY Banyan (Figure 6). The circulation over the eastern North Pacific was dominated by a large cyclonic system over the Aleutian Islands. A relatively weak trough was moving off the East Asia coast to the northwest of TY Banyan. Twelve hours later at 1200 UTC 25 July (Figure 9), TY Banyan continued to propagate to the north as the subtropical ridge continued to be weakened by the cyclonic circulation moving to the east. The shortwave trough over the East Asian coast had advanced over the Sea of Japan and began to approach TY Banyan.

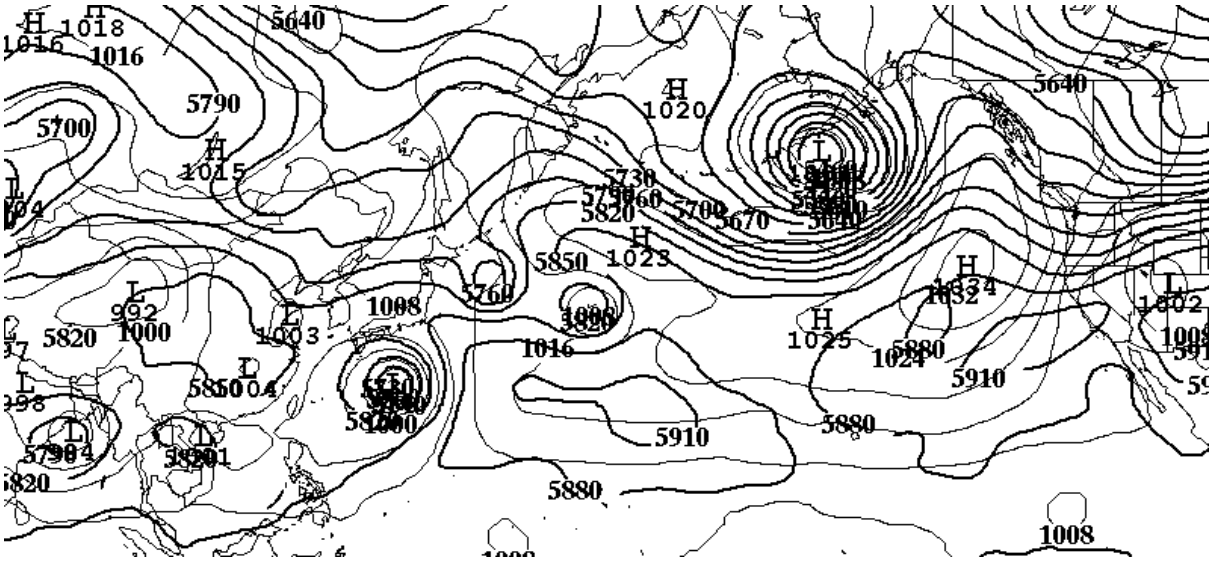

Figure 8. Sea-level pressure (4 hPa interval, thin lines) and 500 hPa heights (30 m interval, thick lines) at 0000 UTC 25 July.

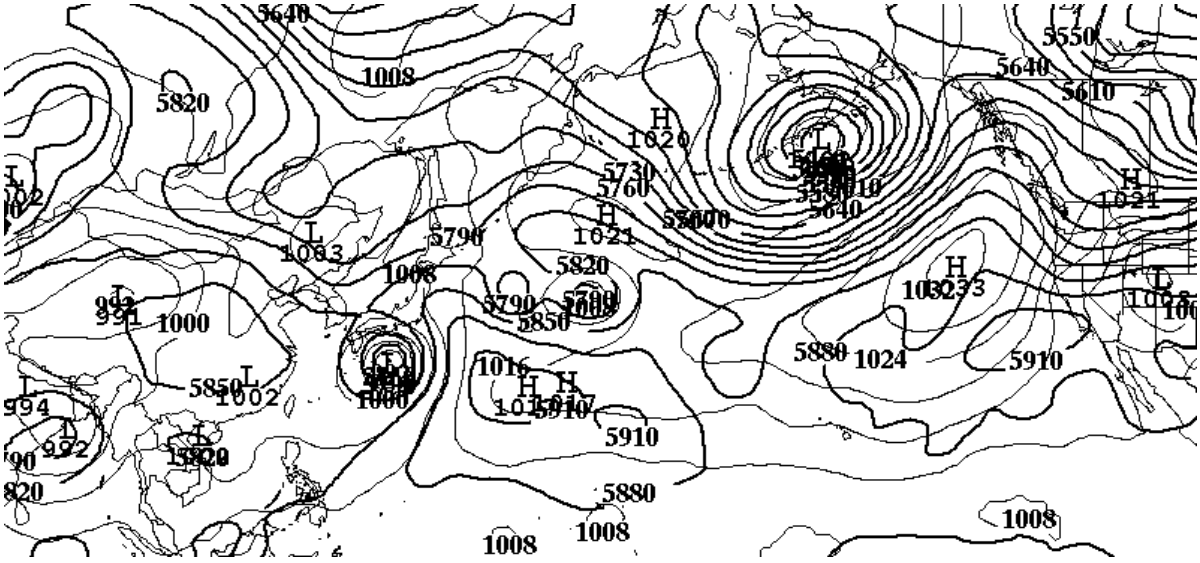

Figure 9. Same as Figure 8, except for 1200 UTC 25 July.

By 0000 UTC 26 July (Figure 10), the subtropical ridge weakened enough to allow TY Banyan to begin recurvature (Figure 6). The trough to the northwest of Banyan became nearly fully aligned with the tropical cyclone. At 1200 UTC 26 July (Figure 11), TY Banyan continued to recurve and became fully imbedded in the shortwave trough propagating off the Asian coast. The relative positioning of the tropical and midlatitude circulations was indicative of the start of the transformation stage of ET (Klein et al. 2000).

Klein et al. (2000) stated that the transformation stage of an ET event typically lasts between 36 and 42 hours. In this case, Typhoon Banyan was classified as an extratropical cyclone at 0000 UTC 28 July 2005 (Figures 6 and 7), which defines a 36-h duration for the transformation stage.

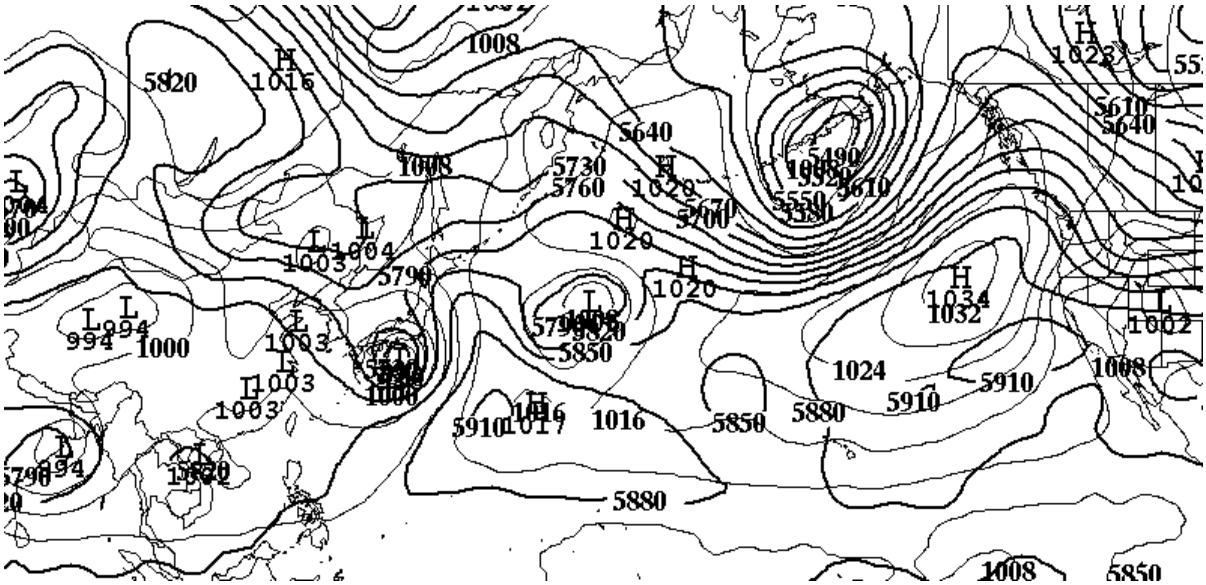

Figure 10. Same as Figure 8, except for 0000 UTC 26 July.

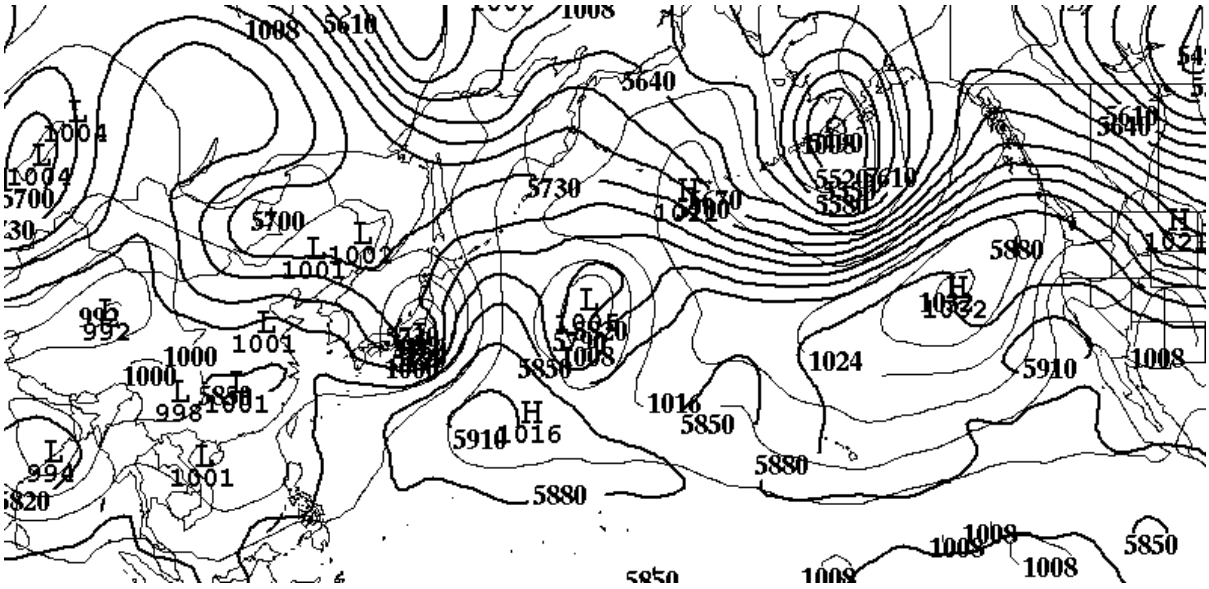

Figure 11. Same as Figure 8, except for 1200 UTC 26 July.

2. Upper-tropospheric Interactions

At 0000 UTC 25 July (Figure 12), it was clear that there was a relative 200 hPa wind maximum associated with the midtropospheric cyclonic circulations to the northeast of Banyan, and a second 200 hPa jet streak was over the East Asia coastline associated with the 500 hPa trough.

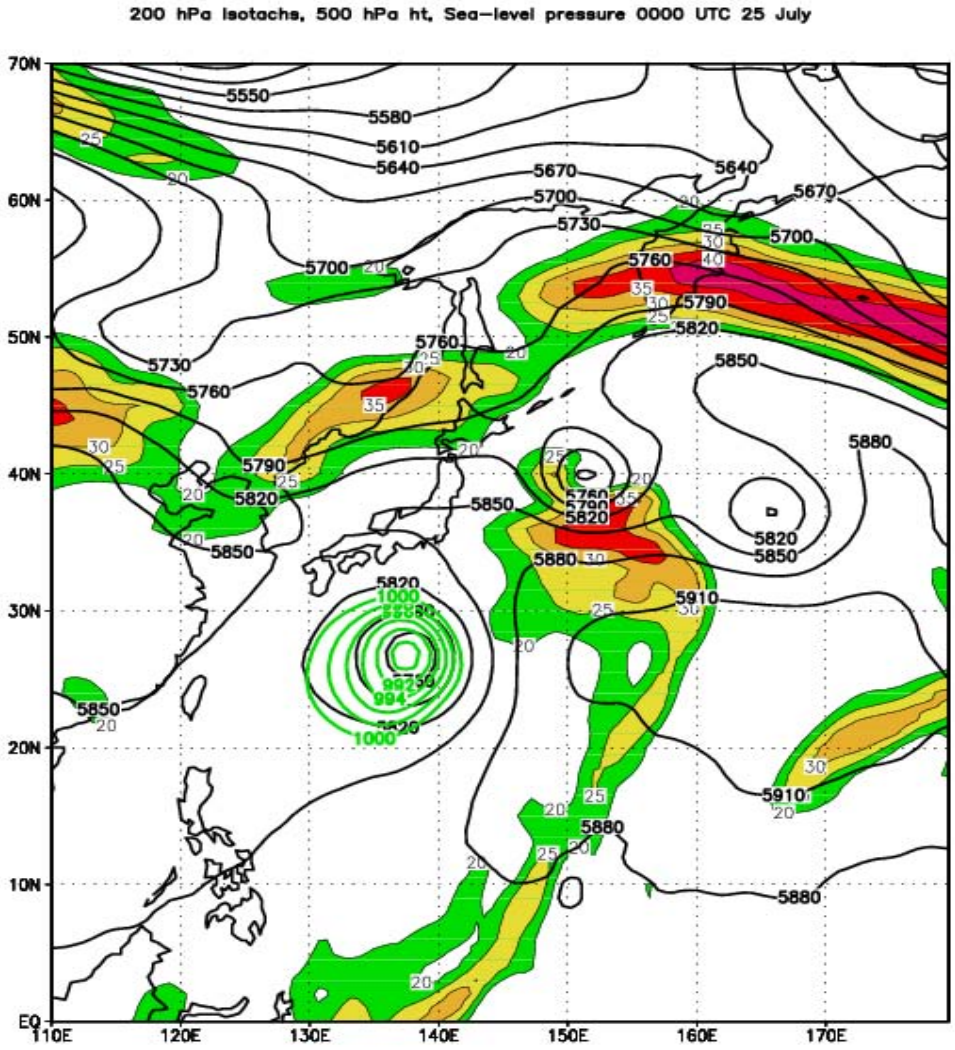

Figure 12. Isotachs at 200 hPa (shaded, m s^{-1}), 500 hPa height (30 m interval), and sea-level pressures ≤ 1000 hPa (green contours, 2 hPa interval) for 0000 UTC 25 July.

At 0600 UTC 25 July (Figure 13), a connection between the outflow of Banyan and the local jet maximum associated with the midtropospheric cyclones to the northeast became evident.

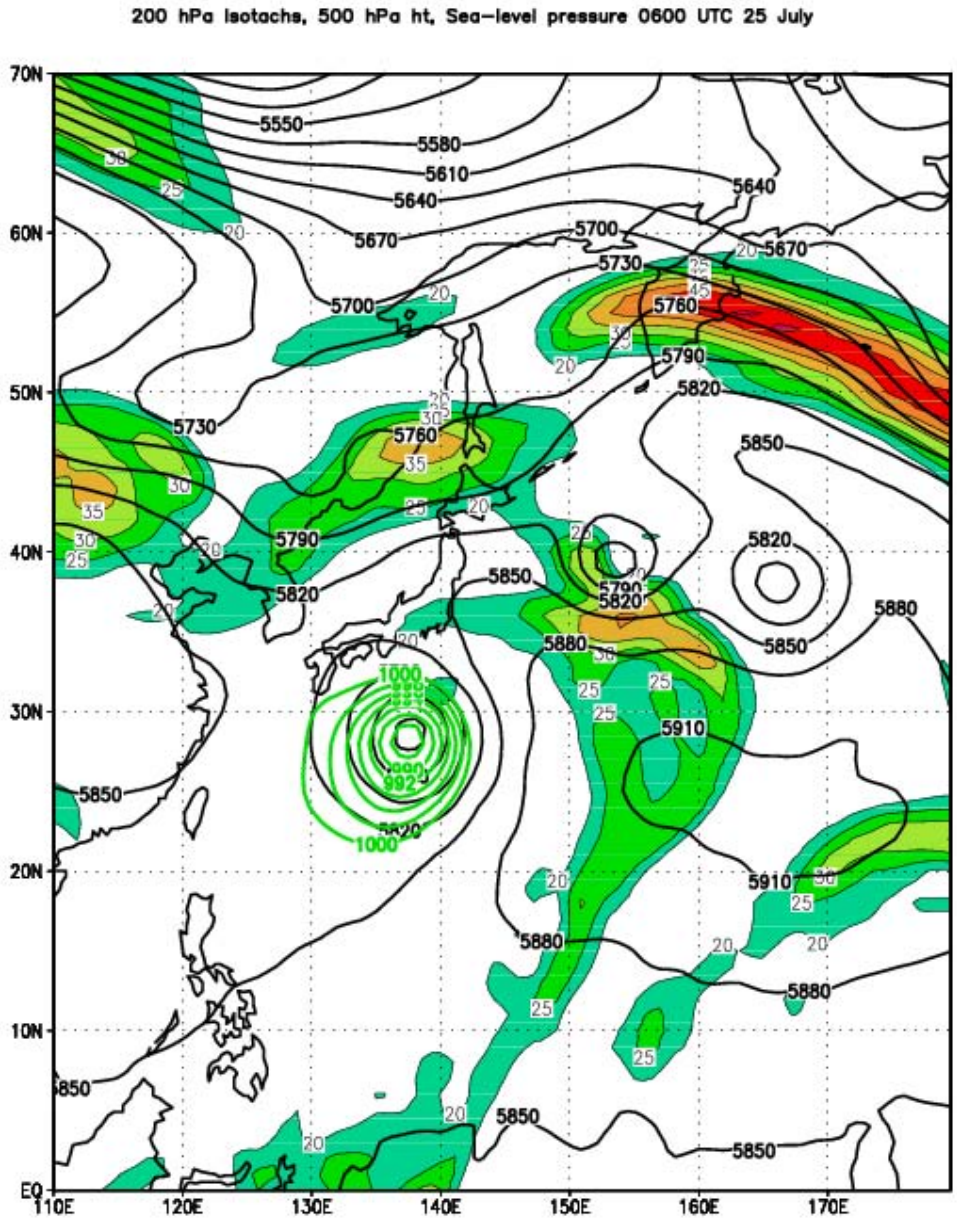

Figure 13. Same as Figure 12, except for 0600 UTC 25 July.

The right-entrance region of this localized jet maximum acts to enhance the upward vertical motion in the eastern quadrants of TY Banyan, which will be discussed later in association with the thermodynamic changes in the decaying tropical cyclone during ET.

By 1200 UTC 25 July (Figure 14), the interaction between the outflow of Banyan and the localized jet has become more evident. The outflow from Banyan has a pronounced anticyclonic curvature as it extends toward the midtropospheric low to the east. The outflow maintains this curvature even though it is approaching the right-entrance region of the separate midlatitude jet, which has a more zonal orientation. The pronounced anticyclonically curved outflow from TY Banyan associated with the midtropospheric low to the east coincides with a northward extension of the subtropical ridge (Figure 15).

The continued northward motion of TY Banyan at 0000 UTC 26 July (Figure 16) initiates the merger between the outflow from the tropical cyclone and the midlatitude jet streak to the north. The outflow region of TY Banyan continues to exhibit pronounced anticyclonic curvature in association with the midtropospheric low to the east. By 0600 UTC 26 July (Figure 17) the outflow of Banyan and the East Asia shortwave trough jet streak have combined to form a single wind maximum exceeding 50 m s^{-1} north of the tropical cyclone. However, the downstream outflow continues to curve anticyclonically toward the midtropospheric cyclone, while the midlatitude jet maintains a zonal orientation. Furthermore, the

subtropical ridge continues to build northward between the TC and the 500 hPa low to the east (Figure 17).

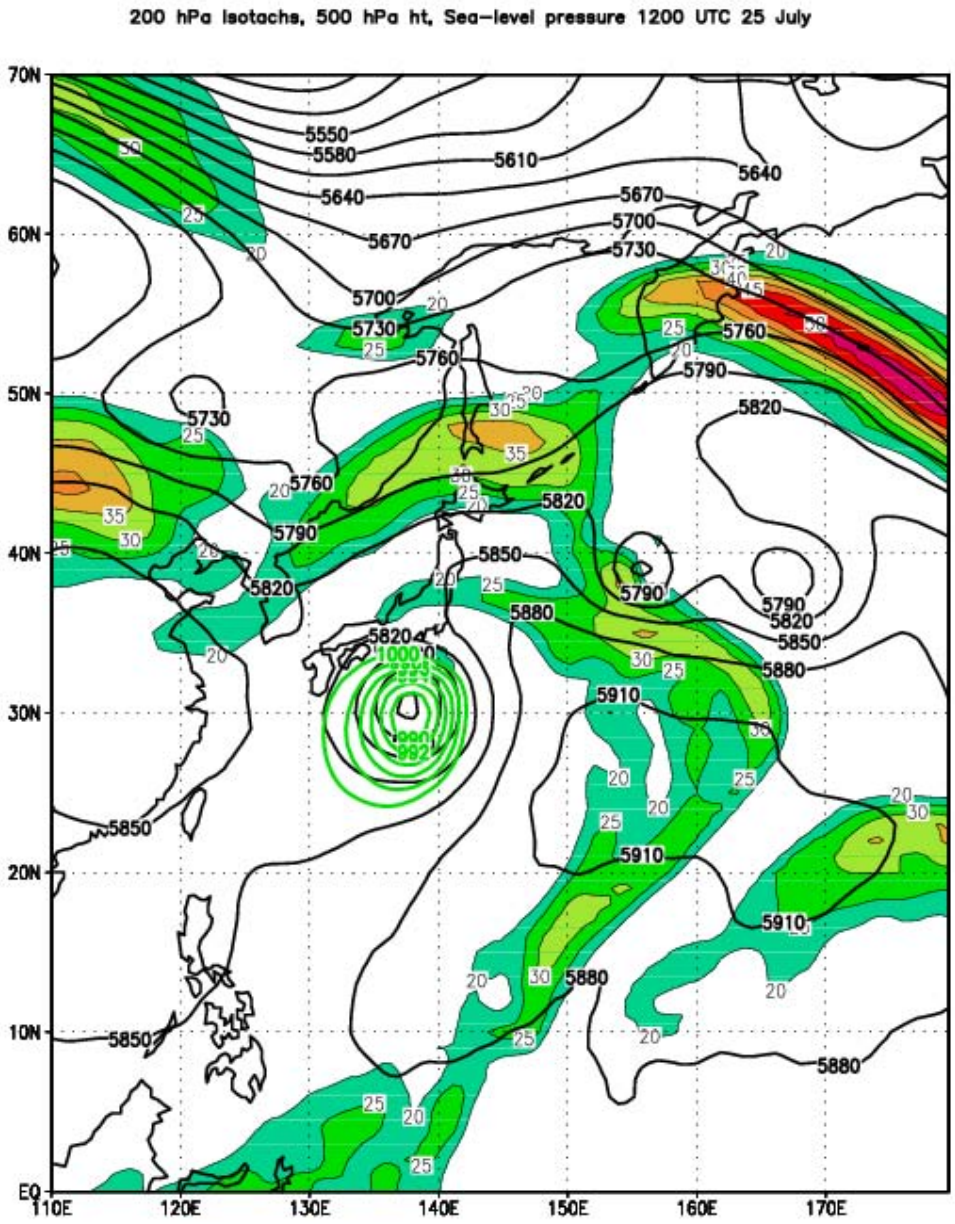

Figure 14. Same as Figure 12, except for 1200 UTC 25 July.

By 1200 UTC 26 July (Figure 18), the TC outflow and midlatitude jet streak have fully merged. The decaying tropical cyclone is now fully under the influence of the right-entrance region of the jet streak, which will be examined in conjunction with the forcing of vertical motion north of Banyan.

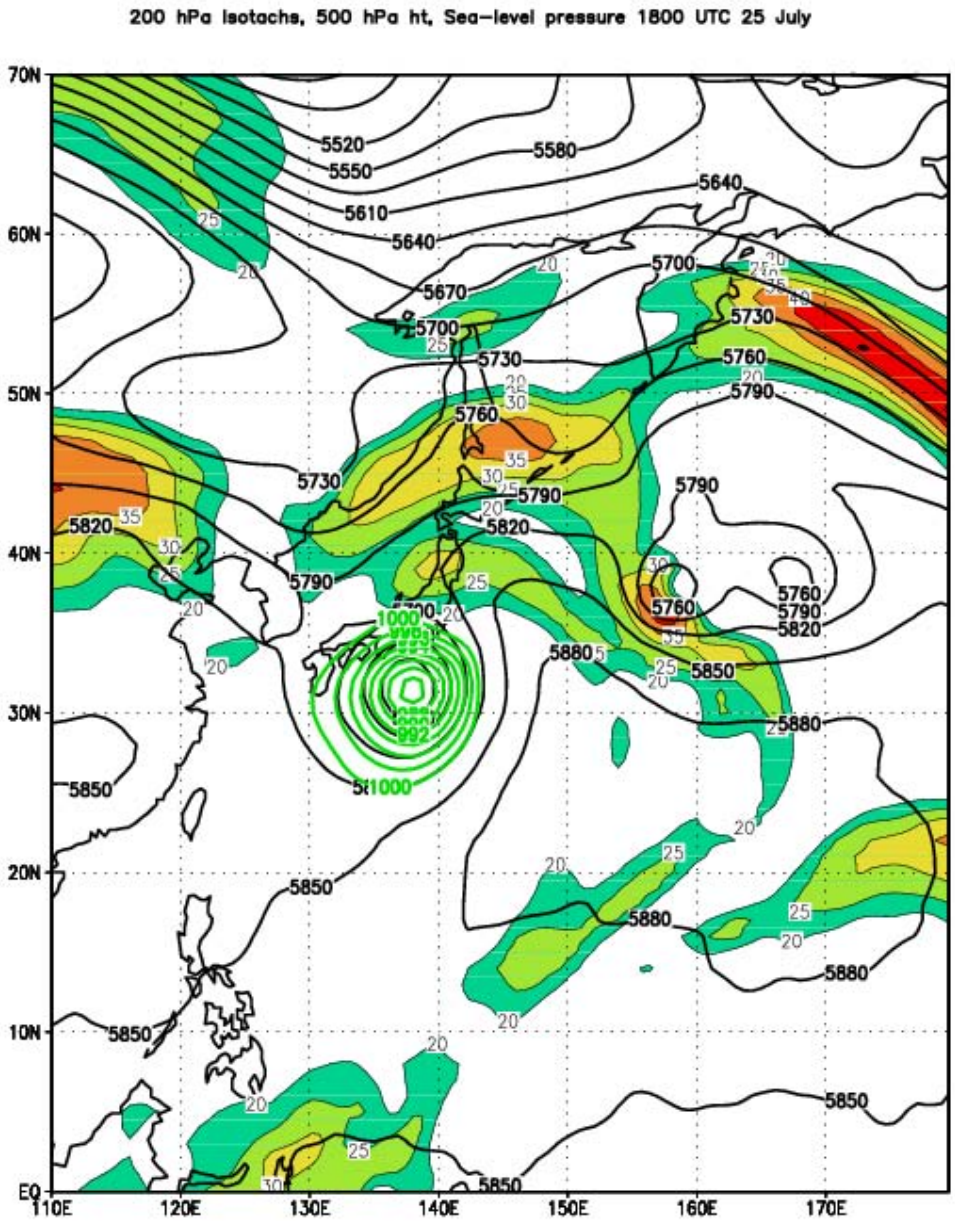

Figure 15. Same as Figure 12, except for 1800 UTC 25 July.

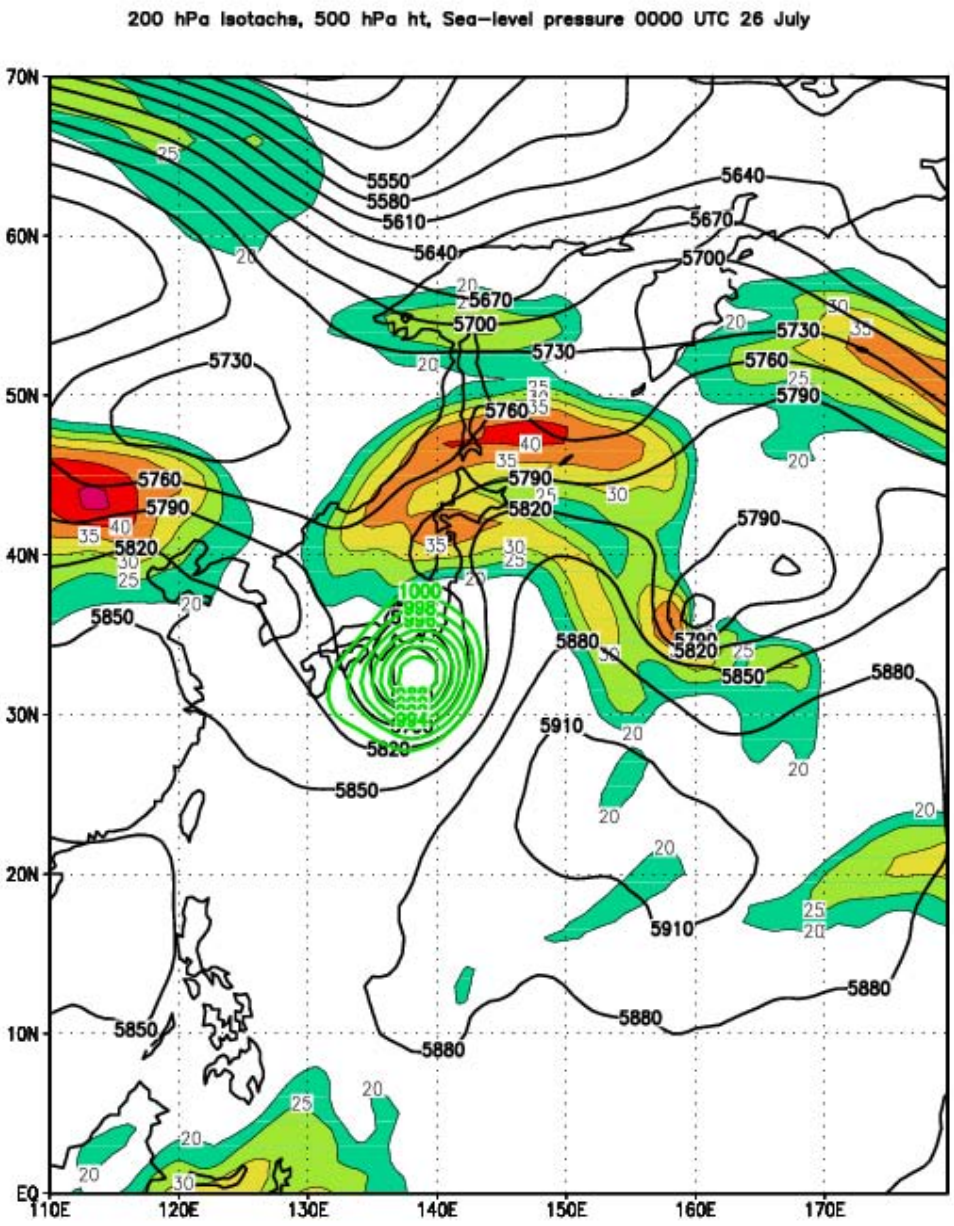

Figure 16. Same as Figure 12, except for 0000 UTC 26 July.

The merger of the outflow and jet streak greatly enhances wind speeds in the jet streak from a maximum of approximately 40 m s^{-1} at 0000 UTC 26 July (Figure 16) to over 55 m s^{-1} at 1800 UTC 26 July (Figure 19). Furthermore,

the merger results in a single jet streak that exhibits strong anticyclonic curvature toward the midtropospheric cyclone to the east of Banyan.

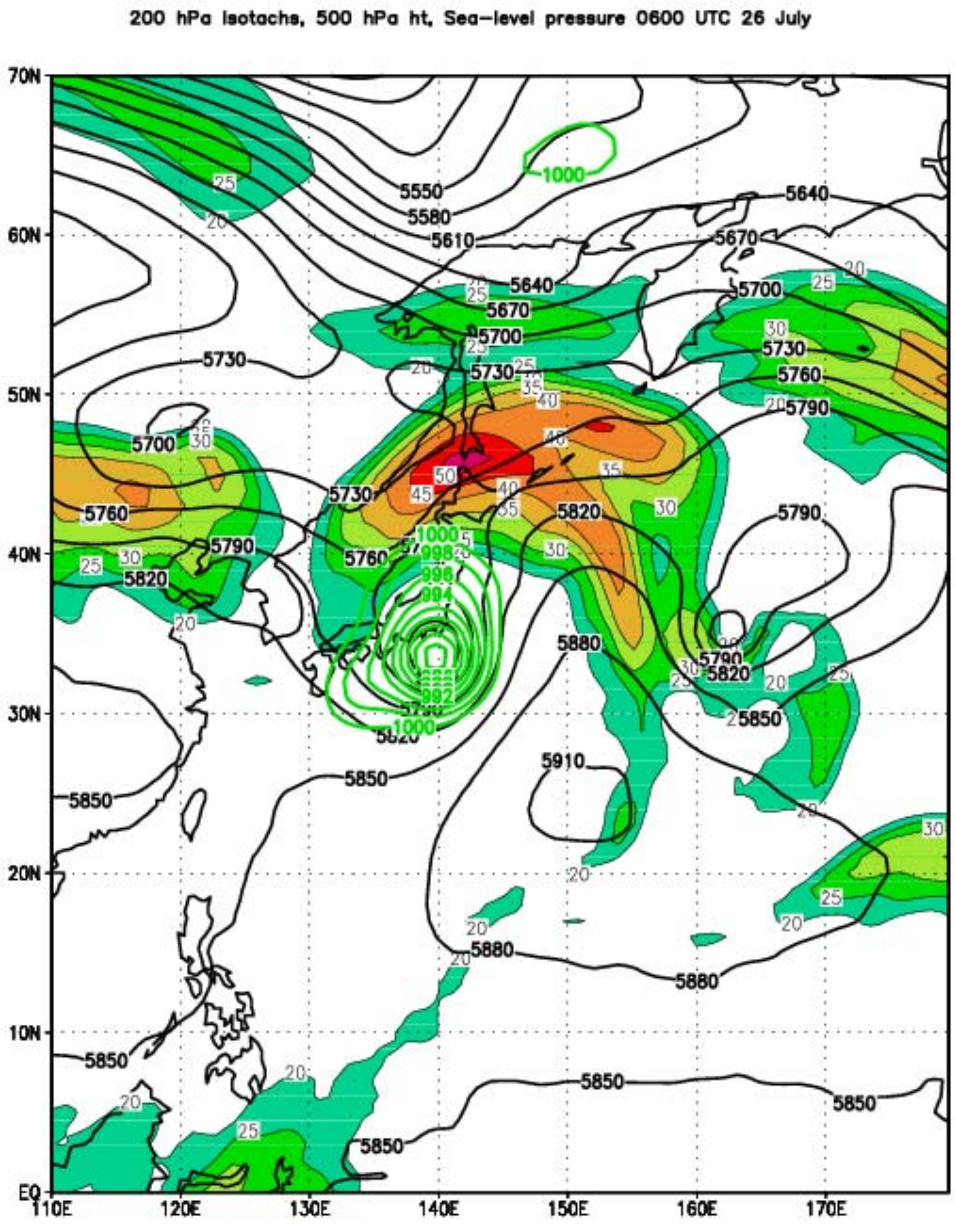

Figure 17. Same as Figure 12, except for 0600 UTC 26 July.

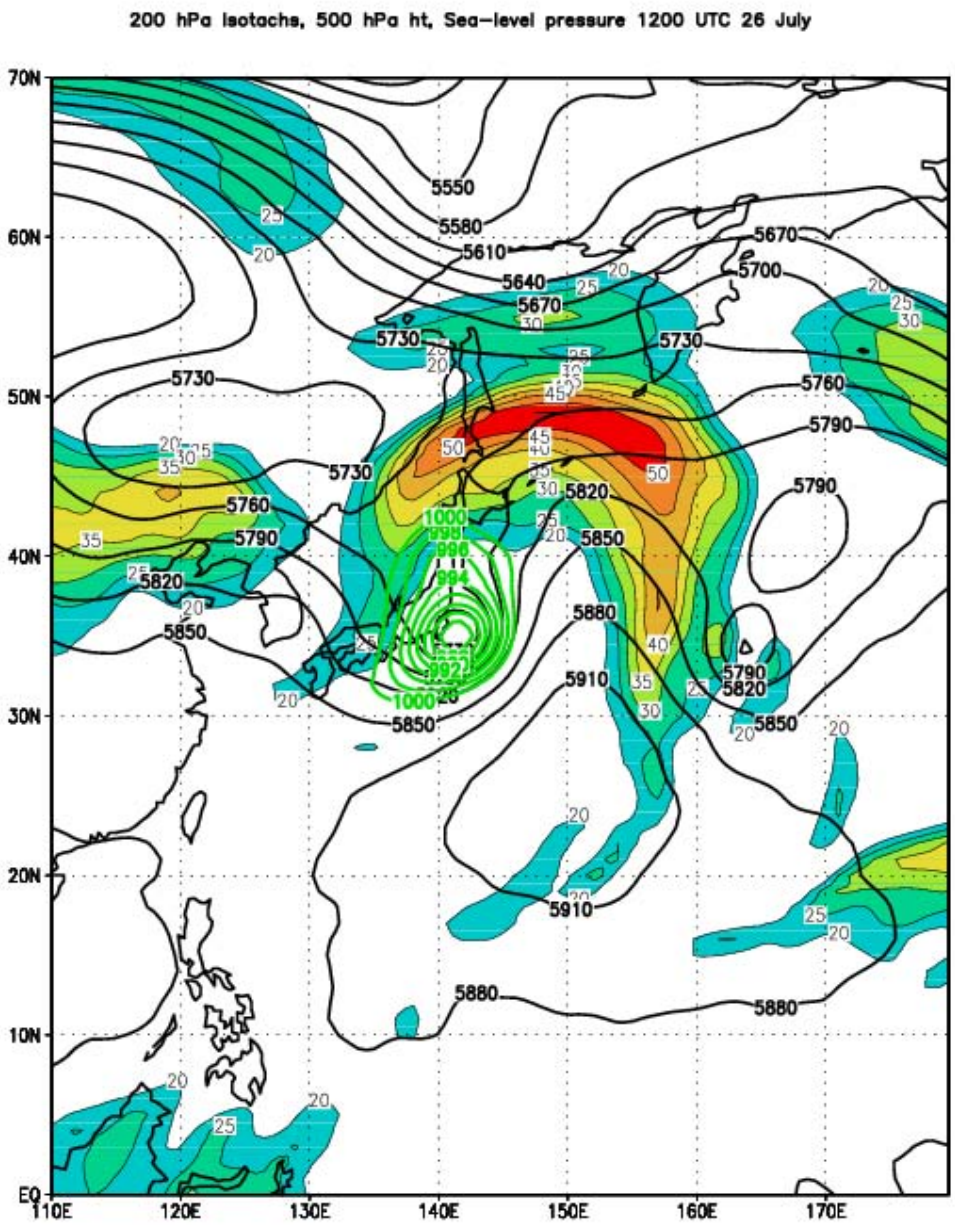

Figure 18. Same as Figure 12, except for 1200 UTC 26 July.

The enhanced jet streak remained to the north as the decaying Banyan moved poleward to become embedded into the midlatitude trough (Figures 20 and 21). The anticyclonic curvature of the jet streak is maintained as Banyan moves

northward and the midtropospheric cyclone to the east digs southward at 1200 UTC (Figure 22) and 1800 UTC (Figure 23) 27 July.

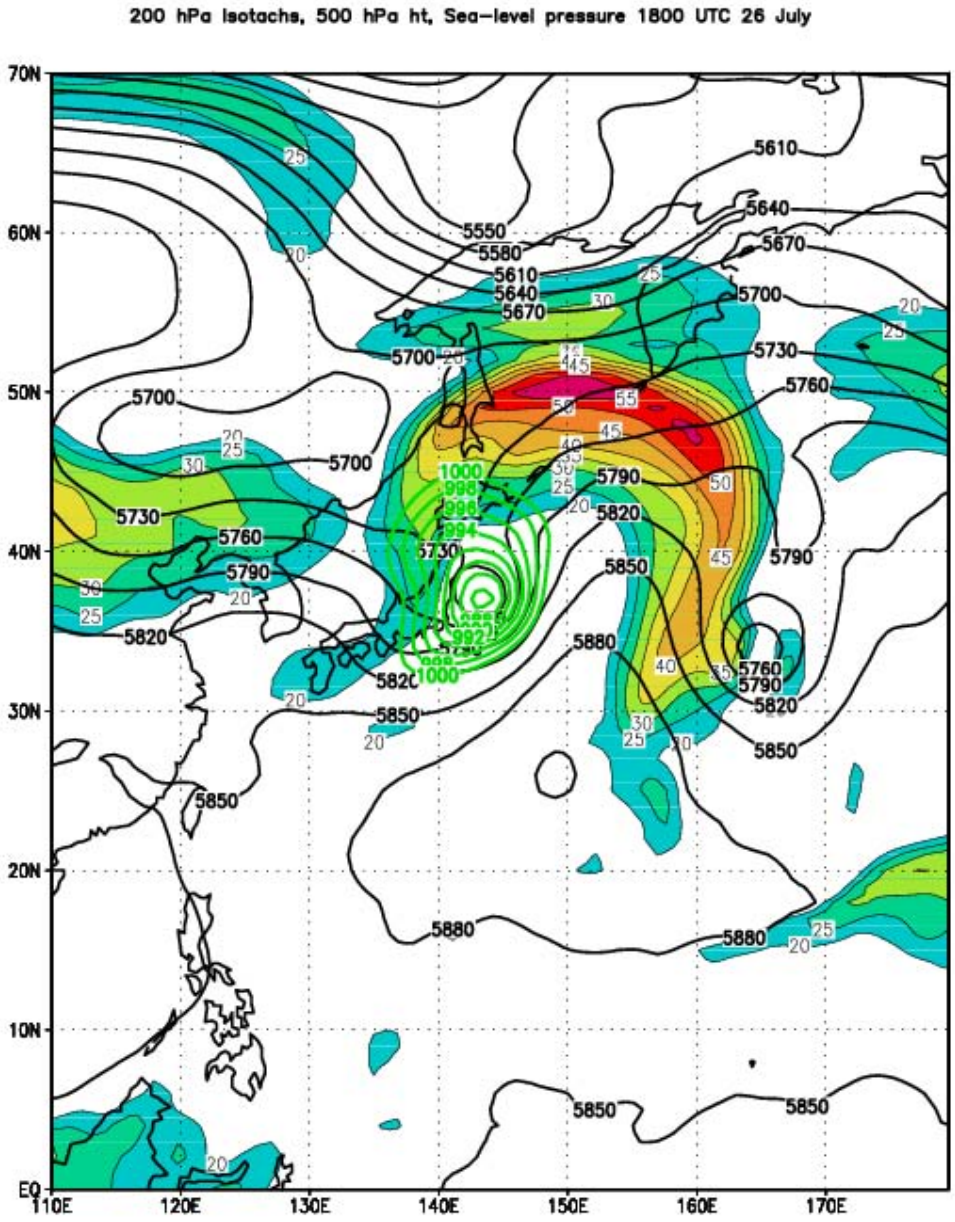

Figure 19. Same as Figure 12, except for 1800 UTC 26 July.

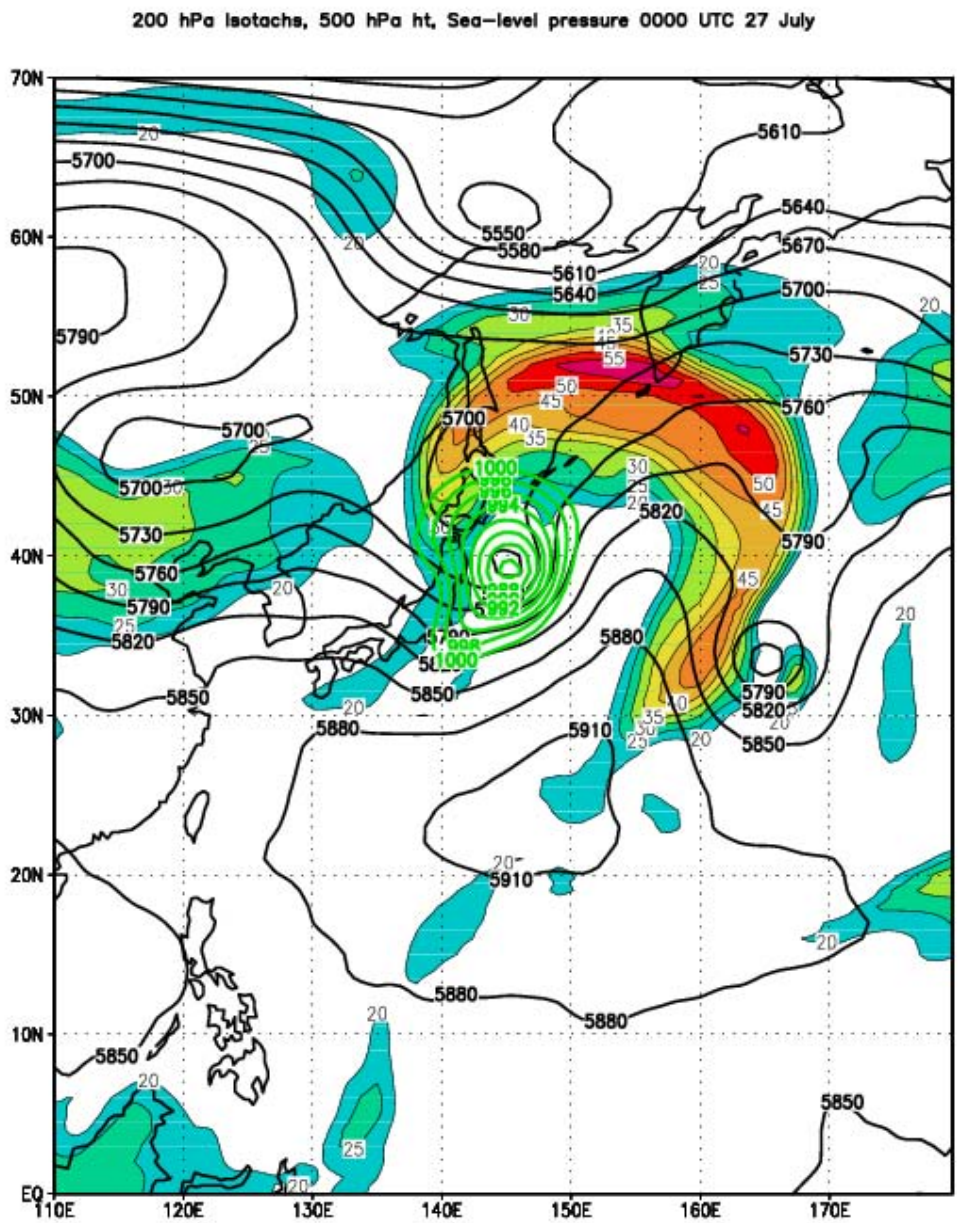

Figure 20. Same as Figure 12, except for 0000 UTC 27 July.

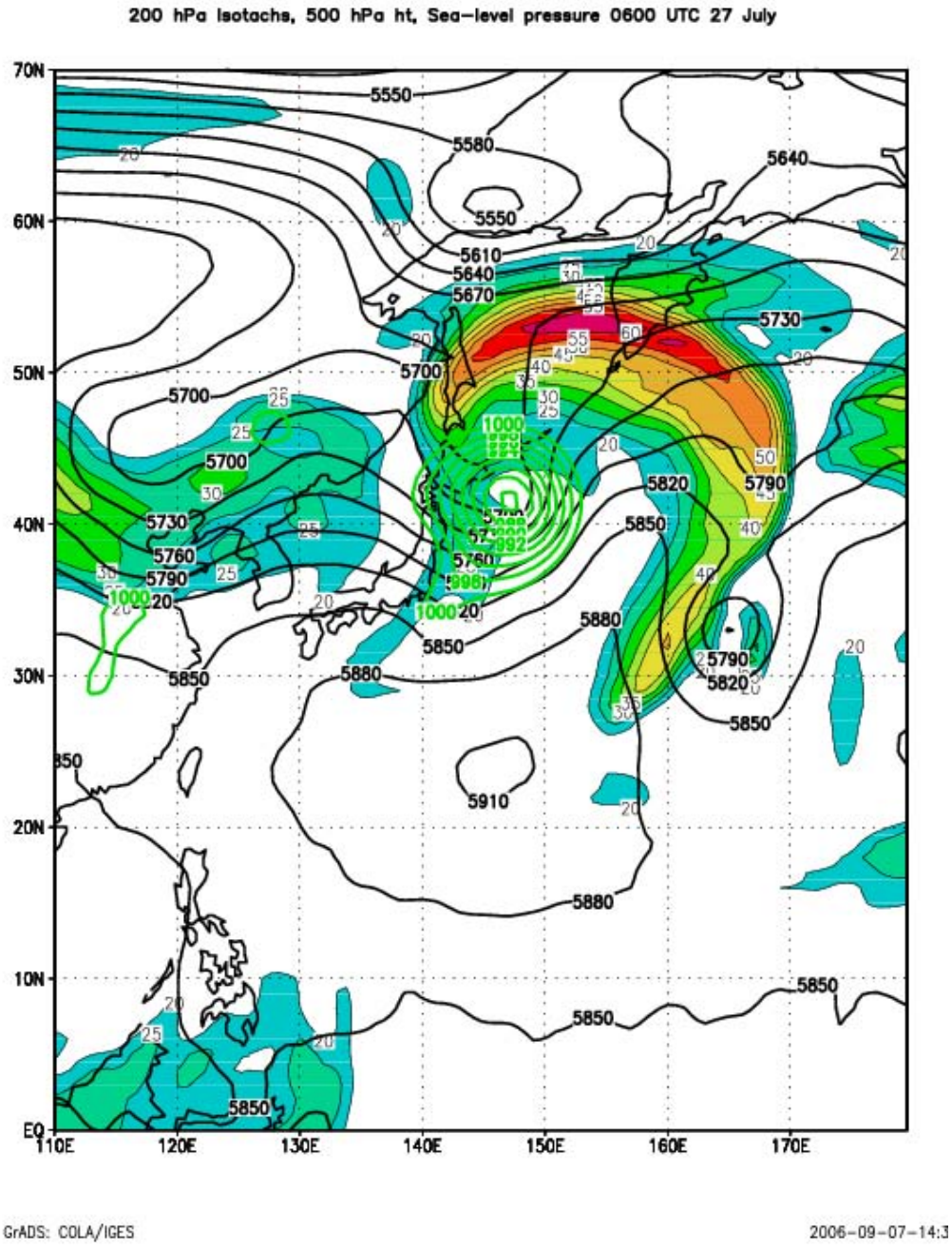

Figure 21. Same as Figure 12, except for 0600 UTC 27 July.

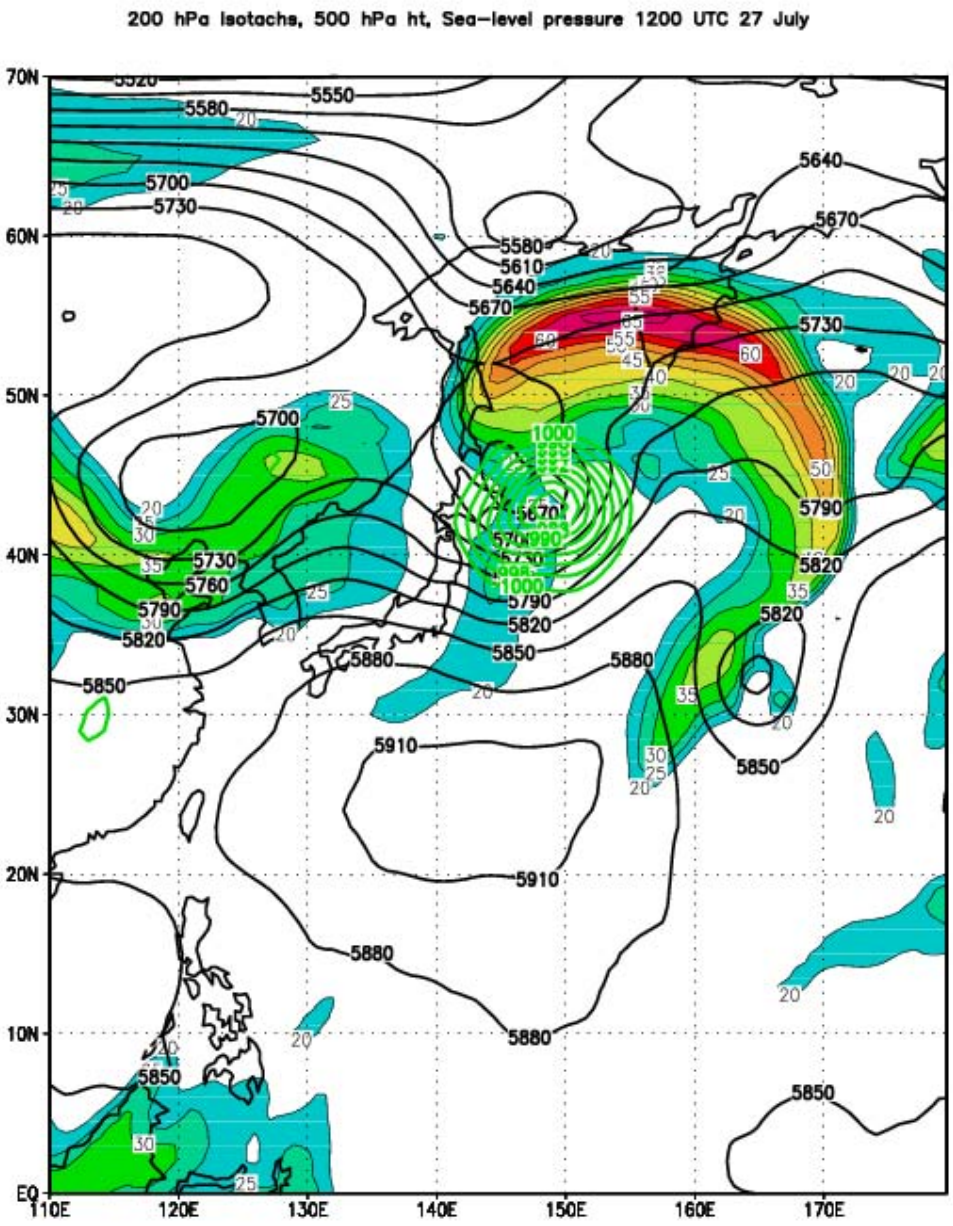

Figure 22. Same as Figure 12, except for 1200 UTC 27 July.

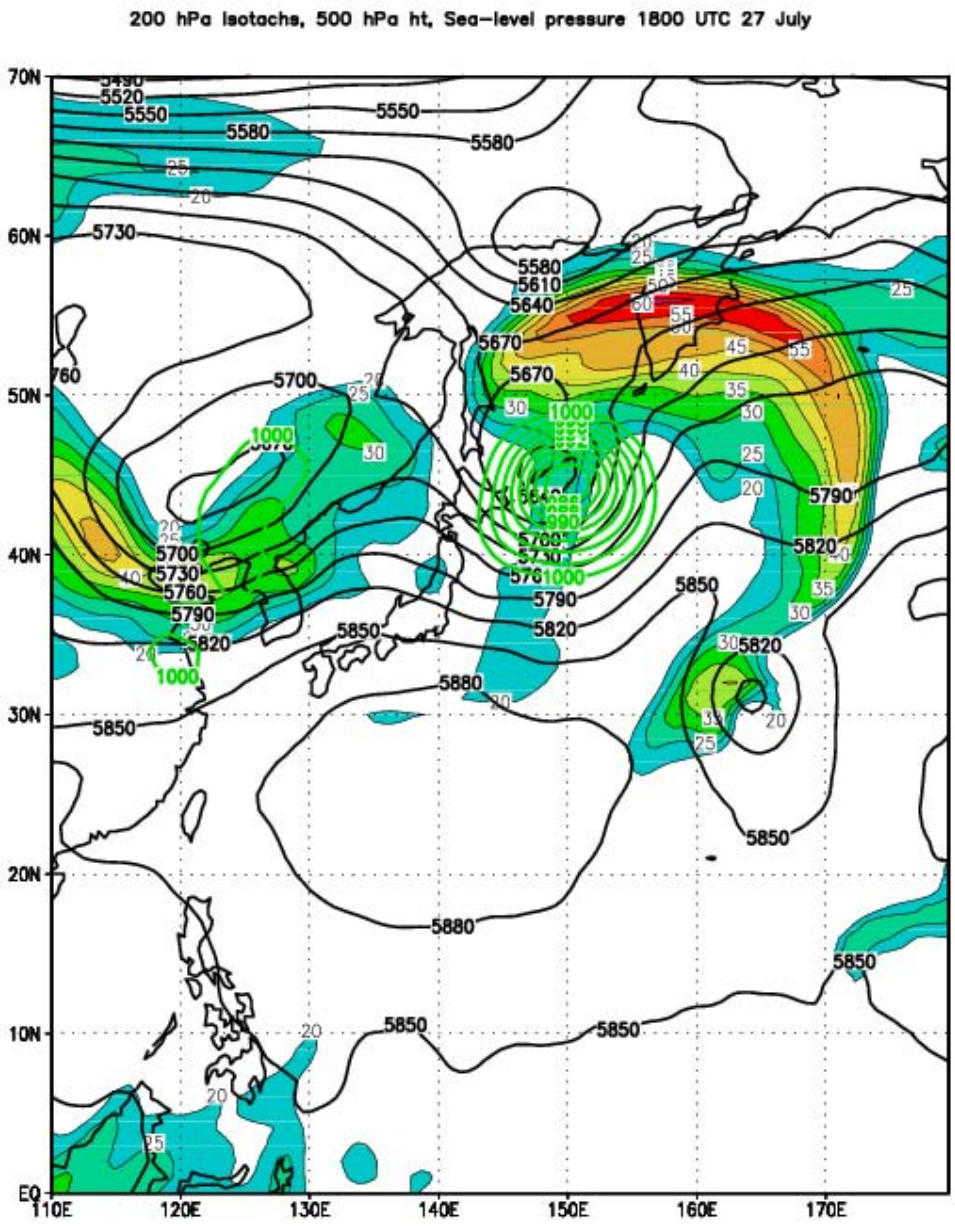

Figure 23. Same as Figure 12, except for 1800 UTC27 July.

In summary, as TY Banyan entered the transformation stage of ET a clear interaction occurred between the outflow of the decaying tropical cyclone circulation and a midtropospheric cyclone to the east and a midlatitude jet streak to the north. The outflow first curved

anticyclonically toward the cyclone to the east, while the jet had a initial zonal orientation. Following the merger of the outflow and the midlatitude jet, the now single jet maximum exhibited strong anticyclonic curvature into the midtropospheric cyclone. The curvature became accentuated as Banyan moved northward and the cyclonic circulation drifted southward. This jet interaction coincided with a pronounced northward extension of the subtropical ridge. To examine the processes associated with the northward extension of the subtropical ridge, the dynamic and thermodynamic conditions associated with the transformation of Banyan are identified in the following section.

B. DYNAMIC AND THERMODYNAMIC EVOLUTION

The dynamic evolution of the transformation of TY Banyan is examined using the distribution of potential vorticity (PV). Potential vorticity is defined on constant isobaric surfaces as:

$$\overline{PV} = -g\left[\overline{\zeta_p} + f + (\vec{k} \times \frac{\partial \vec{\overline{V}}}{\partial \theta})\right]\frac{\partial \theta}{\partial p} \qquad (3.1)$$

where g is the gravitational acceleration, $\overline{\zeta}_p$ is a layer-average relative vorticity on a pressure surface, f is the Coriolis parameter, $\vec{\overline{V}}$ is the layer-average vector wind, θ is potential temperature, and p is pressure. The PV anomaly is defined by the deviation from the zonal average PV. Potential vorticity is a conserved quantity that can

be redistributed through diabatic processes. Using synoptic-scale gridded fields, the computation of the diabatic influences can be difficult to compute. However, the total derivative of PV can be used to define a proxy for diabatic processes as:

$$\frac{d(\overline{PV})}{dt} = \frac{1}{\rho}(\overline{\zeta} \bullet \nabla \dot{\theta}) \qquad (3.2)$$

where ρ is the density, $\dot{\theta}$ is the diabatic heating, and the overbar represents the layer average.

A tropical cyclone is represented by a large deep vertically-upright region of positive PV, which is transported poleward during ET. As the storm undergoes ET, cold advection begins in the western quadrants of the storm, while warm advection occurs in the eastern quadrants. The warm, moist air that is advected around the eastern side of the storm is associated with rising motion. The warm advection and upward vertical motion and associated release of latent heat will contribute to an increase in thickness to the east of the poleward-moving tropical cyclone. In terms of the distribution of PV, the midtropospheric heating maximum on the eastern side of the decaying tropical cyclone will contribute to a *positive* change in the lower-level PV ($\frac{d\left(\overline{PV}\right)}{dt}$>0), and a *negative* change in the upper-level PV ($\frac{d\left(\overline{PV}\right)}{dt}$<0). At the same time, the cold advection occurring on the western side of the storm brings cold, dry air into the storm, which erodes the convection and eventually the eye wall convection. This

erosion eventually causes the storm to take on the more asymmetric appearance of an extratropical cyclone.

To diagnose the dynamic evolution of the PV distribution, cross-sections and plan-view diagrams of the PV, PV anomaly, the time derivative of the potential vorticity ($\frac{d\left(\overline{PV}\right)}{dt}$), relative humidity, and vertical motion (ω) are constructed from the gridded analyzed fields. The time tendency of the PV distribution is used to diagnose areas where diabatic heating is influencing the PV distribution at upper and lower levels. Relative humidity and vertical motion are used to indicate the potential for diabatic processes.

The thermodynamic environment during the transformation of Banyan is examined with the Advanced Microwave Sounding Unit. The Demuth et al. (2004) algorithm was used to construct temperature fields in a storm-centered region at synoptic times from 0000 UTC 25 July to 1800 UTC 27 July. Temperature anomalies observed by the AMSU are defined as a difference from the average over the storm-centric region using the Demuth et al. (2004) algorithm. The temperature anomaly fields were used to construct meridional cross-sections at the storm center longitude and two degrees east and west of the storm center. Zonal cross-sections were also constructed at the storm center and in intervals of one degree latitude to three degrees north of the storm. Due to the limitations of revisit time on polar orbiting satellites, few satellite overpasses occur directly at synoptic times. This limitation is partially alleviated by grouping overpasses

with the synoptic time closest to the overpass, resulting in a maximum time differential between the satellite overpass and the synoptic time of three hours. For those synoptic times without a satellite overpass within the three hour window temperature retrievals were not available. In this study there were no satellite overpasses within three hours of synoptic times 0600 UTC 26 July, or 0600 and 1200 UTC 27 July .

Tropical cyclones bring regions of anomalously warm temperatures, particularly in the upper atmosphere, poleward. For a mature tropical cyclone, warm anomalies typically have an upright structure similar to that of the PV distribution discussed above. The peak warm anomaly occurs in the upper atmosphere. The amount of the anomalous warming may be related to the intensity of the tropical cyclone, with stronger storms having higher peak anomaly temperatures. Although, the anomaly in a mature tropical cyclone is typically centered over the storm, the process of ET can result in a significant down-shear tilt of the temperature distribution.

The PV structure of the mature tropical cyclone at 0600 UTC 25 July (Figure 24a) is an upright column of large PV. The time tendency of PV is dominated by variations at upper levels. To the west of the center an upper-level positive tendency is associated with the approach of the shortwave over the East Asia coast. Negative values over the center are associated with the outflow of Banyan, while the positive values at upper levels to the east of the storm center are associated with the upper-level cyclones to the east of Banyan.

At 0600 UTC 25 July, a large area of high relative humidity and upward vertical motion exists east of the center of Banyan. To the west of Banyan, the air is considerably drier, with very little vertical motion. Accordign to the AMSU retrievals, anomalously warm air extended down to the surface (Figures 24c, d). A relative maximum in low-level temperature to the east of the tropical cyclone center was related to the warm, moist air being advected around Banyan to the east of the center.

The distribution of PV remains fairly consistent between 0600 UTC (Figure 24a) and 1800 UTC 25 July (Figure 25a). However, regions of positive and negative PV tendency are beginning to appear centered near 500 hPa to the east and west of the tropical cyclone. The west-east vertical distribution of vertical motion and relative humidity have changed dramatically between 0600 UTC (Figure 24b) and 1800 UTC (Figure 25b). Sinking motion is found west and near the center of Banyan and the maximum rising motion is to the east. The distribution of relative humidity also reveals a strong west-east asymmetry. Related to the asymmetric vertical motion and relative humidity fields is a distortion in the west-east temperature anomaly profile (Figure 25d). The low-level warm temperature anomaly occurs to the east (Figure 25d) and north (Figure 25c) of the storm center, while the upper-level warm anomaly remains over the center of Banyan.

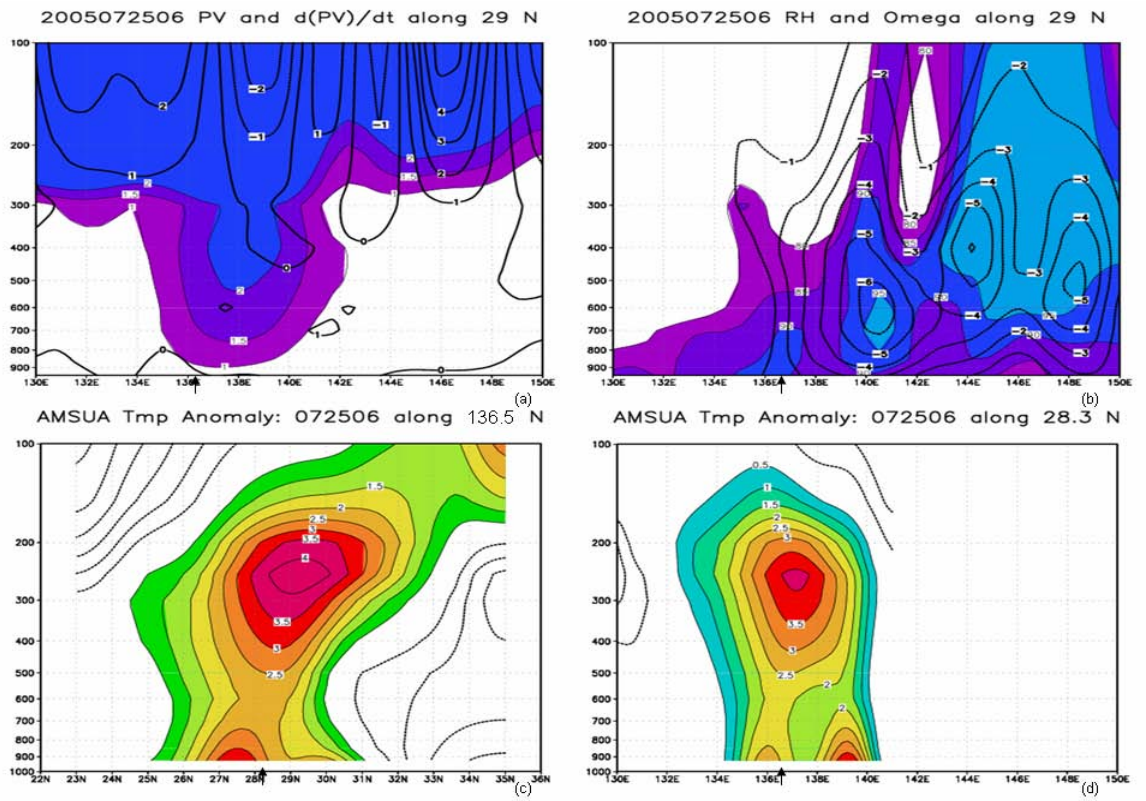

Figure 24. Zonal cross section at 0600 UTC 25 July along 29°N for (a) PV (shaded, 1 PVU = 10^{-6} K m^2 kg^{-1} s^{-1}) and the time tendency of PV (lines, 1 PVU s^{-1}), and (b) omega (lines, 1 μb s^{-1} interval) and relative humidity (percent, shaded > 80%). Temperature anomalies (K) retrieved from AMSU-A are contained in a (c) meridional cross-section along 136.5°E and (d) zonal cross-section along 28.3°N. The arrows along the abscissa indicate the position of the TC.

By 0000 UTC 26 July (Figure 26a), the region of positive $\frac{d\left(\overline{PV}\right)}{dt}$ had increased in the midtroposphere on the eastern side of the tropical cyclone. The distribution of vertical motion (Figure 26b) becomes more axisymmetric than it was 6 h earlier. However, a region of descending air is

found to the west of the storm center (Figure 26b). The temperature anomalies (Figures 26c, 26d) at 0000 UTC 26 July have become concentrated over the storm center at low and upper levels. A warm anomaly does spread south (Figure 26c) and east (Figure 26d) of the storm center. Therefore, between 1800 UTC 25 July and 0000 UTC 26 July the circulation of Banyan seems to have become more symmetric and more upright. This may be in response to a period of reduced vertical wind shear.

By 1200 UTC 26 July (Figure 27), several important features can be noted, and it is from this time in the ET event that a more detailed description will be given in the following sections. The upper-level trough that propagates off the coast of East Asia is now evident to the west of Banyan (Figure 27a) as a descending lobe of high PV. Furthermore, an area of positive $\frac{d\left(\overline{PV}\right)}{dt}$ at upper levels just to the west of the storm center in Figure 27a is associated with the trough that is moving off the East Asia coast. A broad region of subsiding air is to the west of the center of Banyan (Figure 27b), and there is a distinct eastward tilt to the distribution of vertical motion. The asymmetric profile of vertical motion, combined with the high relative humidity to the east of the storm occurs in an area of maximum low-level temperature anomaly the east of storm center (Figure 27 d). Because the upper-troposphere warm anomaly remains over the storm center (Figures 27c, d) there is a distinct east-to-west tilt in

the vertical distribution of temperature (Figure 27d). There is also a southern extension of low level warming (Figure 27c).

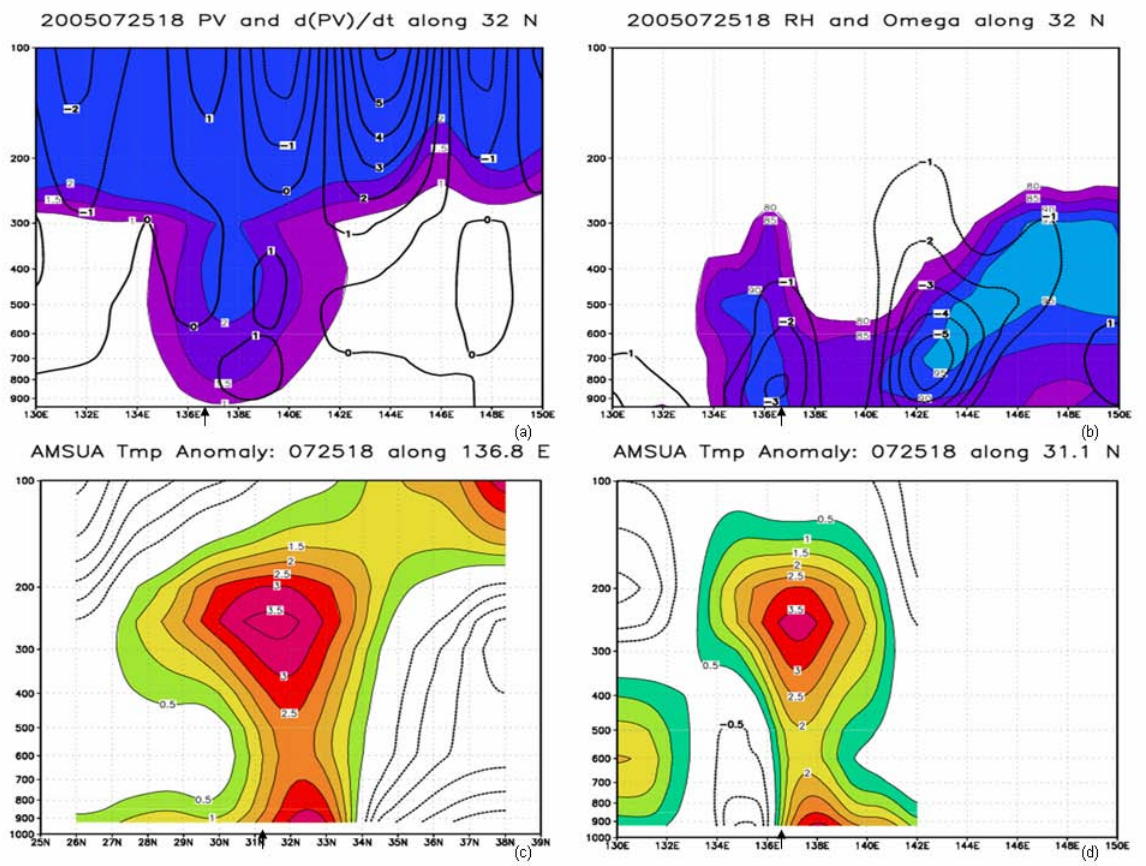

Figure 25. As in Figure 24, except for 1800 UTC 25 July, cross-sections for (a) and (b) along 32°N, (c) along 136.8°E and (d) along 31.1°N.

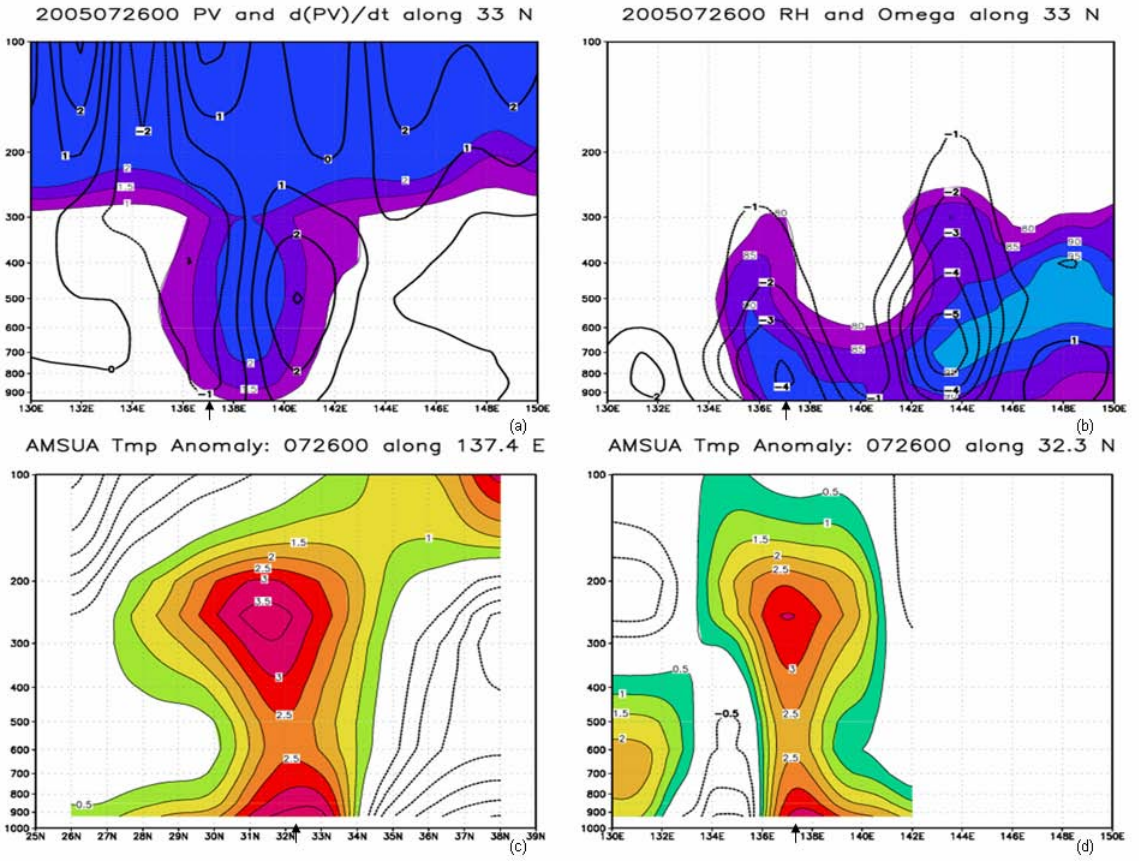

Figure 26. As in Figure 24, except for 0000 UTC 26 July, cross-sections for (a) and (b) along 33°N, for (c) along 137.4°E and for (d) along 32.3°N.

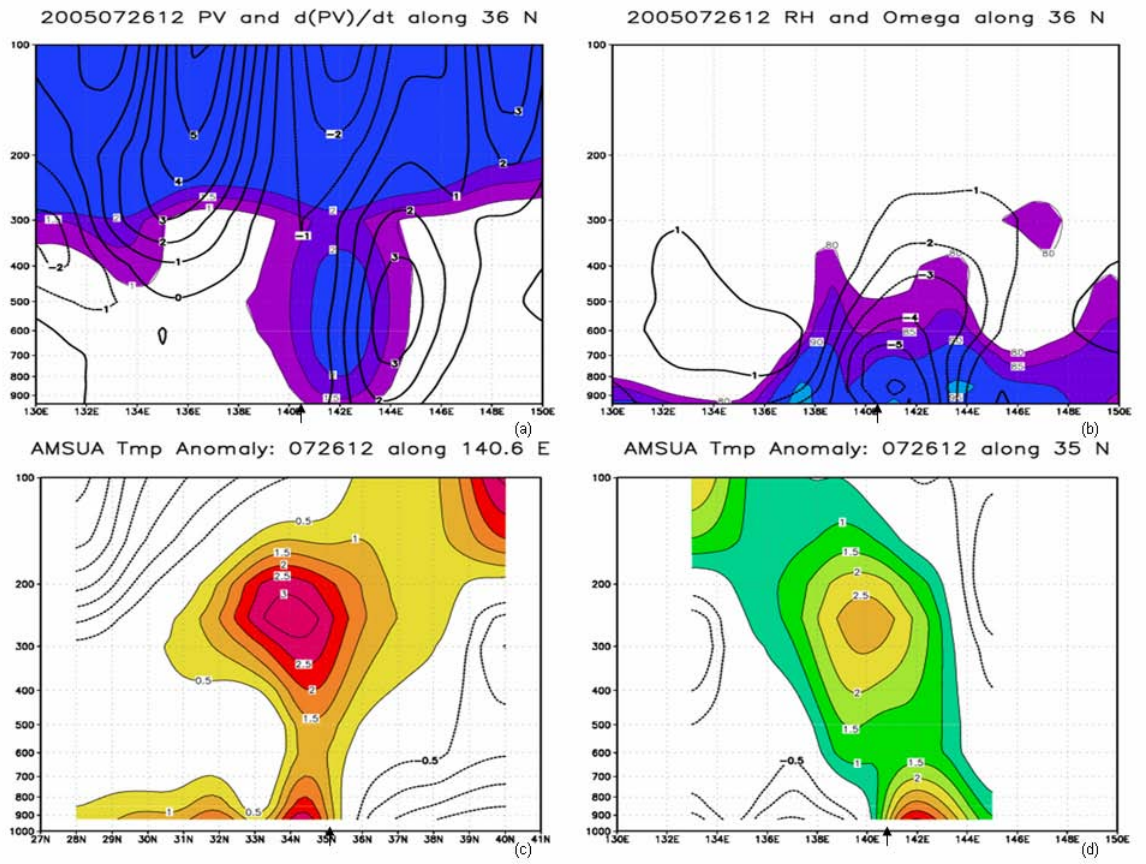

Figure 27. As in Figure 24, except for 1200 UTC 26 July, cross-sections for (a) and (b) along 36°N, for (c) along 140.6°E, and for (d) along 35°N.

At 1800 UTC 26 July (Figure 28a), the area of upper-level positive $\frac{d\left(\overline{PV}\right)}{dt}$ to the west of Banyan extends downward to the midtroposphere as the midlatitude trough approaches the decaying tropical cyclone. A large area of dry air exists to the west of the storm center with some subsidence (Figure 28b). The distribution of vertical motion to the east of the storm center remains tilted toward the east. A northward tilt (Figure 28c) is now apparent in the upper-

level temperature anomaly. However, the warm anomaly through the entire troposphere has been shifted to the east of the center of Banyan (Figure 28d).

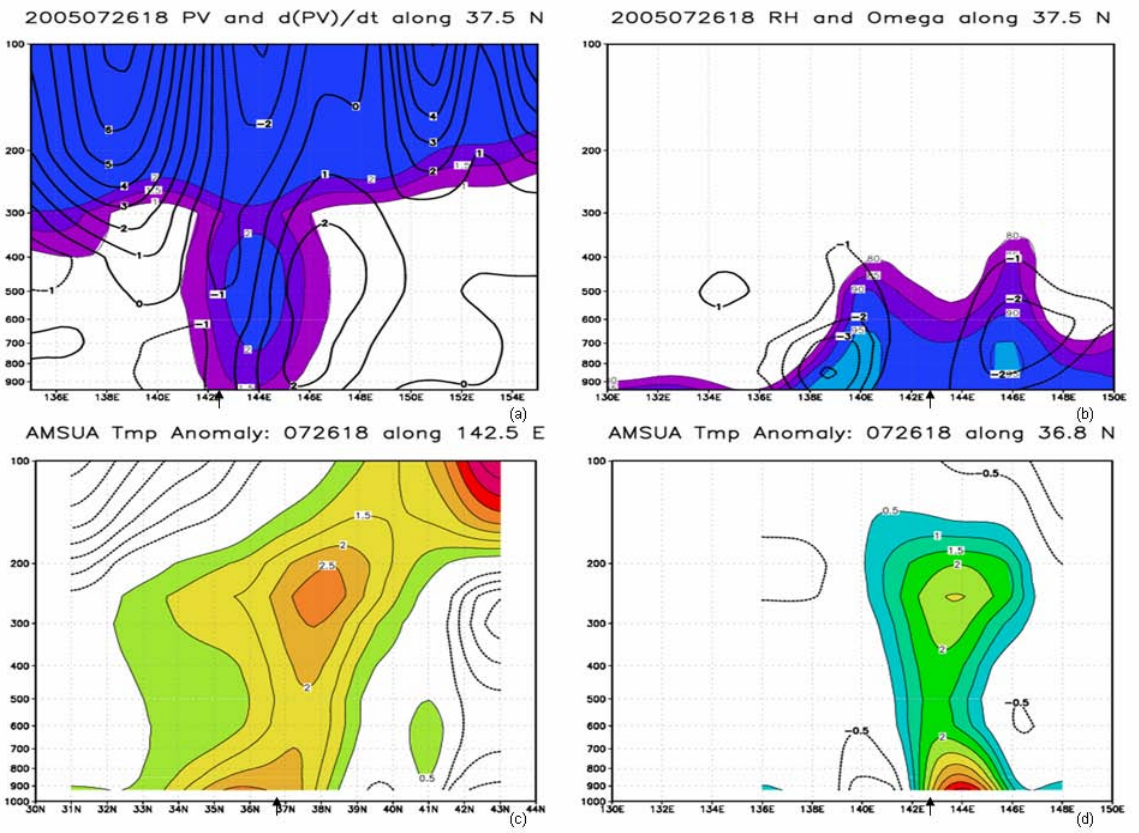

Figure 28. As in Figure 24, except for 1800 UTC 26 July, cross-sections for (a) and (b) along 37.5°N, for (c) along 142.5°E, and for (d) along 36.8°N.

Significant changes in the distribution of PV, time tendency of PV, and temperature distribution now occur in the 6 h between 1800 UTC 26 July (Figure 28) and 0000 UTC 27 July (Figure 29a). As the upper-level trough approaches Banyan from the west, the region of positive PV time tendency is nearly adjacent to Banyan, and the distribution of PV in the midtroposphere has begun to extend westward

toward the upper-level trough. The area of positive time tendency of PV to the east of Banyan has deepened in the vertical and become tilted toward the east in the middle and upper troposphere. The region of negative time tendency of PV at upper levels also extends to the east over the region of midtropospheric positive PV tendency. At low levels, the distribution of vertical motion is distinctly tilted to the east (Figure 29b). Both the low-level and upper-level maximum warm anomalies are shifted to the south of the storm center, with an extension of the low-level warm anomaly to the north of center (Figure 29c). The low-level temperature anomaly at the storm center may be caused by rainfall contamination. The intrusion of cooler air to the west of the storm is clearly defined by the AMSU-A temperature data (Figure 29d).

By 1800 UTC 27 July (Figure 30), Typhoon Banyan has taken on characteristics common to the end of the transformation stage of ET (Klein et al. 2000). The lower-tropospheric PV distribution has a distinct tilt to the east (Figure 30a), before it extends back to the west in the vertical as it merges with the PV of the midlatitude trough. The maximum positive region of $\frac{d\left(\overline{PV}\right)}{dt}$ in the upper levels has moved over the center of the storm as the decaying circulation of Banyan becomes aligned in the midlatitude trough. There are two regions of upward vertical motion (Figure 30b). The maximum upward vertical motion is to the east of the storm center and is associated with the warm advection of moist air associated with the remnant tropical cyclone circulation. A secondary region

of upward vertical motion is centered near 400 hPa to the west of the tropical cyclone center and is associated with forcing by the midlatitude trough. The gradient in the temperature distribution to the north of the storm center marks the location of the warm frontal boundary merging in the upper-troposphere with the residual warm anomaly of the tropical cyclone (Figure 30c). The upward vertical motion associated with the midlatitude trough, in combination with the undercutting by cold air from the west, causes the strong east-to-west tilt in the temperature distribution (Figure 30d).

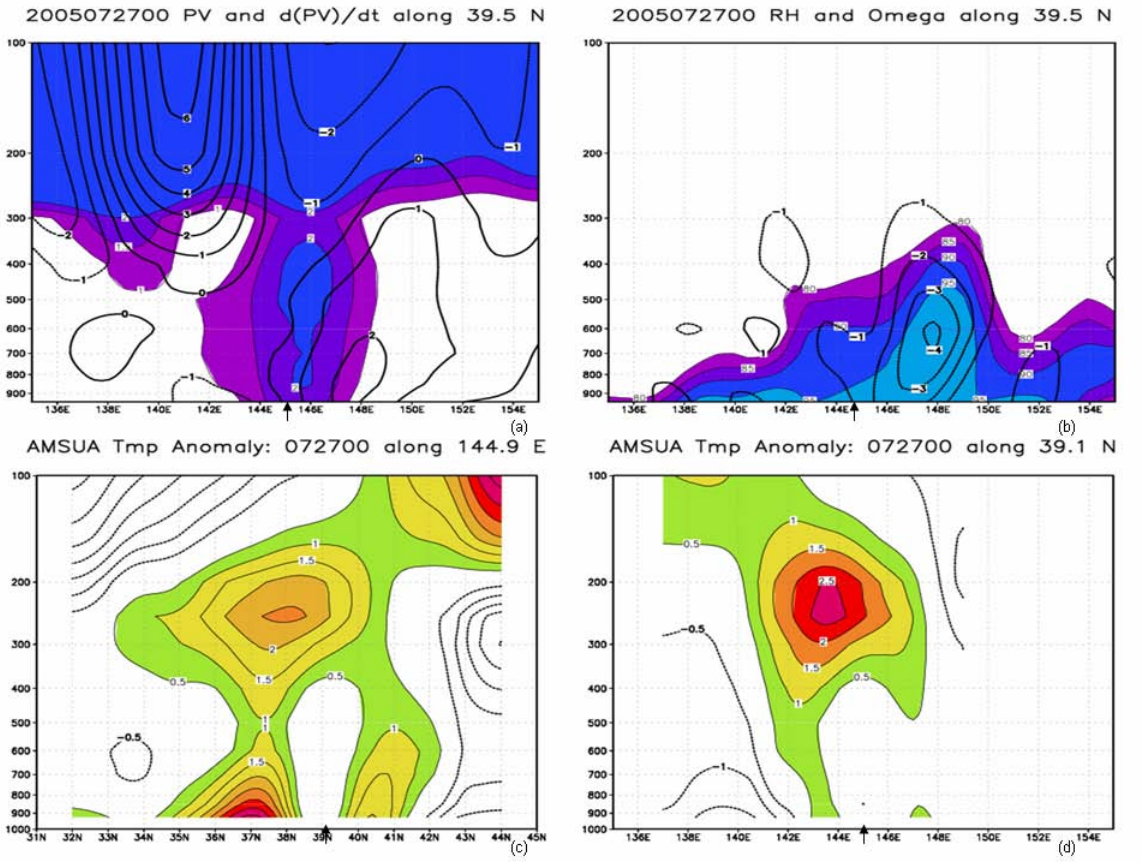

Figure 29. As in Figure 24, except for 0000 UTC 27 July, cross-sections for (a) and (b) along 39.5°N, for (c) along 144.9°E, and for (d) along 39.1°N.

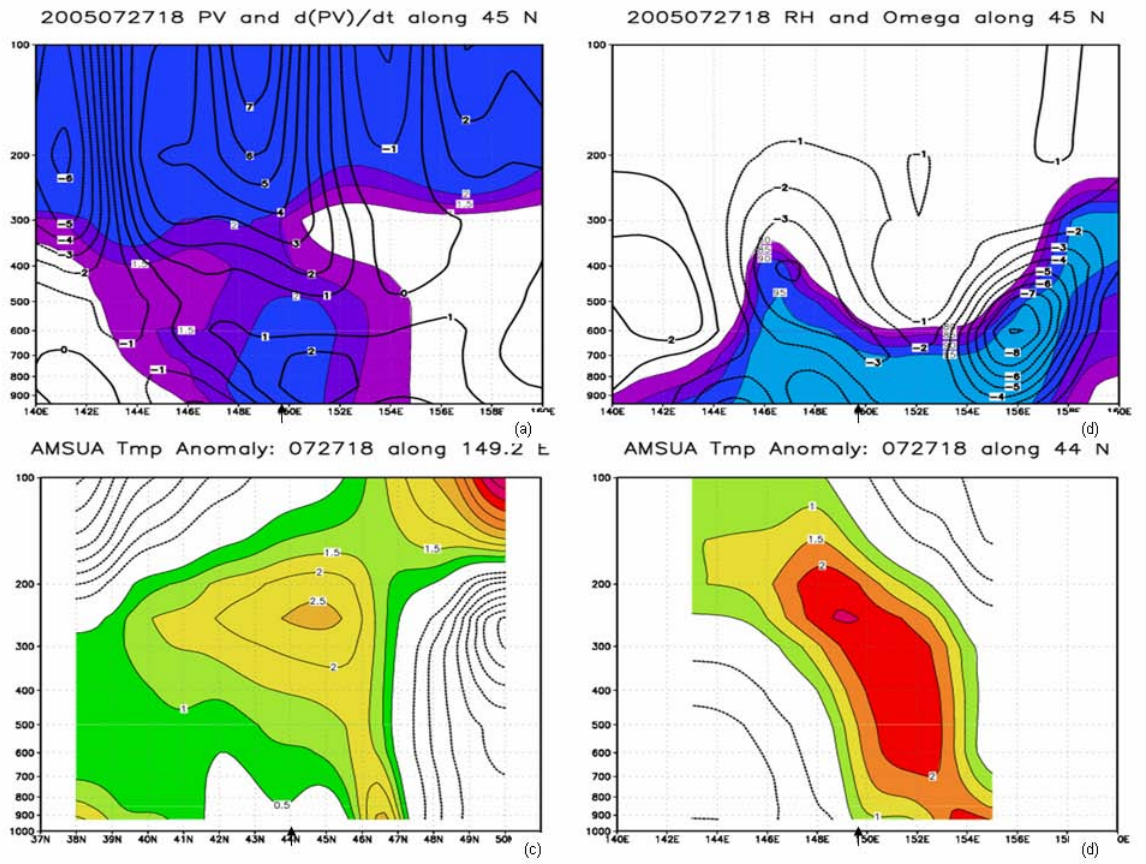

Figure 30. Same as Figure 24, except for 1800 UTC 27 July, cross-sections for (a) and (b) along 45°N, for (c) along 149.2°E, and for (d) along 44°N.

Recall that major changes in the dynamic and thermodynamic structures of Banyan began at 1200 UTC 26 July due to the influence of the upper-level trough to the west and the asymmetric distributions of temperature, moisture, and vertical motion. The complex temperature structure at this time is investigated with plan views of AMSU-A temperature anomalies at 400 hPa (Figure 31a) and 850 hPa (Figure 31b). The vertical distribution of temperature is examined with a meridional cross-section through the center of Banyan (Figure 31c) and two degrees longitude east of the center (Figure 31d). The zonal

distribution of temperature anomaly is examined with a cross-section one degree latitude north (Figure 31e) and two degrees north (Figure 31f) of the storm center. The east-to-west tilt in the temperature distribution in Figure 27d is evident in the plan-view temperature distribution (Figures 31a, b). The maximum warm anomaly in the 400 hPa plan view occurs in a crescent-shaped region over the northern half of the circulation with a maximum to the west of the storm center. The maximum warm anomaly at 850 hPa occurs to the east of storm center. Regions of cold air advection can be seen in both the 400 hPa and 850 hPa plan-view temperature distributions as cool anomaly regions to the west and south wrap cyclonically about the storm center. The upward vertical motion (Figure 27b) to the east of the storm center coincides with a broad, low-level warm anomaly seen in (Figure 31d). A relative warm anomaly occurs to the east at 400 hPa (Figure 31d), which is lower than the relative warm anomaly over the storm center (Figure 31c).

The southward advection of cooler air is defined as the anomalously cool regions to the west of the storm center (Figures 31e, f). Immediately north of the center, the temperature anomaly has a pronounced tilt to the west. At low levels, warm anomalies to the east are associated with the warm-air advection. A mid-level warm anomaly is found over the center in association with the decaying tropical cyclone. This mid-level anomaly has a tilt to the west toward the upper-level warm anomaly, which is near the tropopause in association with the midlatitude trough.

As TY Banyan entered the midlatitudes, it underwent several important dynamic and thermodynamic changes. The shortwave trough moving off the coast of East Asia as well as the mid-tropospheric cyclone to the east, brought regions of positive potential vorticity time tendency into proximity with Banyan. These positive PV time tendency regions interacted with the storm, which eventually caused a downstream tilt to the PV distribution of the storm. The distribution of upward vertical motion underwent dramatic changes under the influence of the midlatitude circulations. The distribution of vertical motion became concentrated to the east of the storm center, and took on a distinct eastward tilt. As the transformation stage was completed, a strong region of upward vertical motion developed farther to the east associated with the remnants of the cyclonic circulation. A secondary upward vertical motion region centered west and over the decaying tropical cyclone center was associated with the trough moving off the coast of East Asia.

The temperature distribution also underwent complex changes. As expected for a mature tropical cyclone, the temperature distribution initially had the maximum warm anomaly in the upper troposphere centered over the storm. Under the influence of the midlatitude circulations, the low-level warm anomaly first shifted to the east and north of the storm center. The temperature distribution eventually took on a distinctive westward and northward tilt. To examine the processes associated with the northward extension of the subtropical ridge, the coupling of the PV anomaly and the upper-level wind field is examined in the following section.

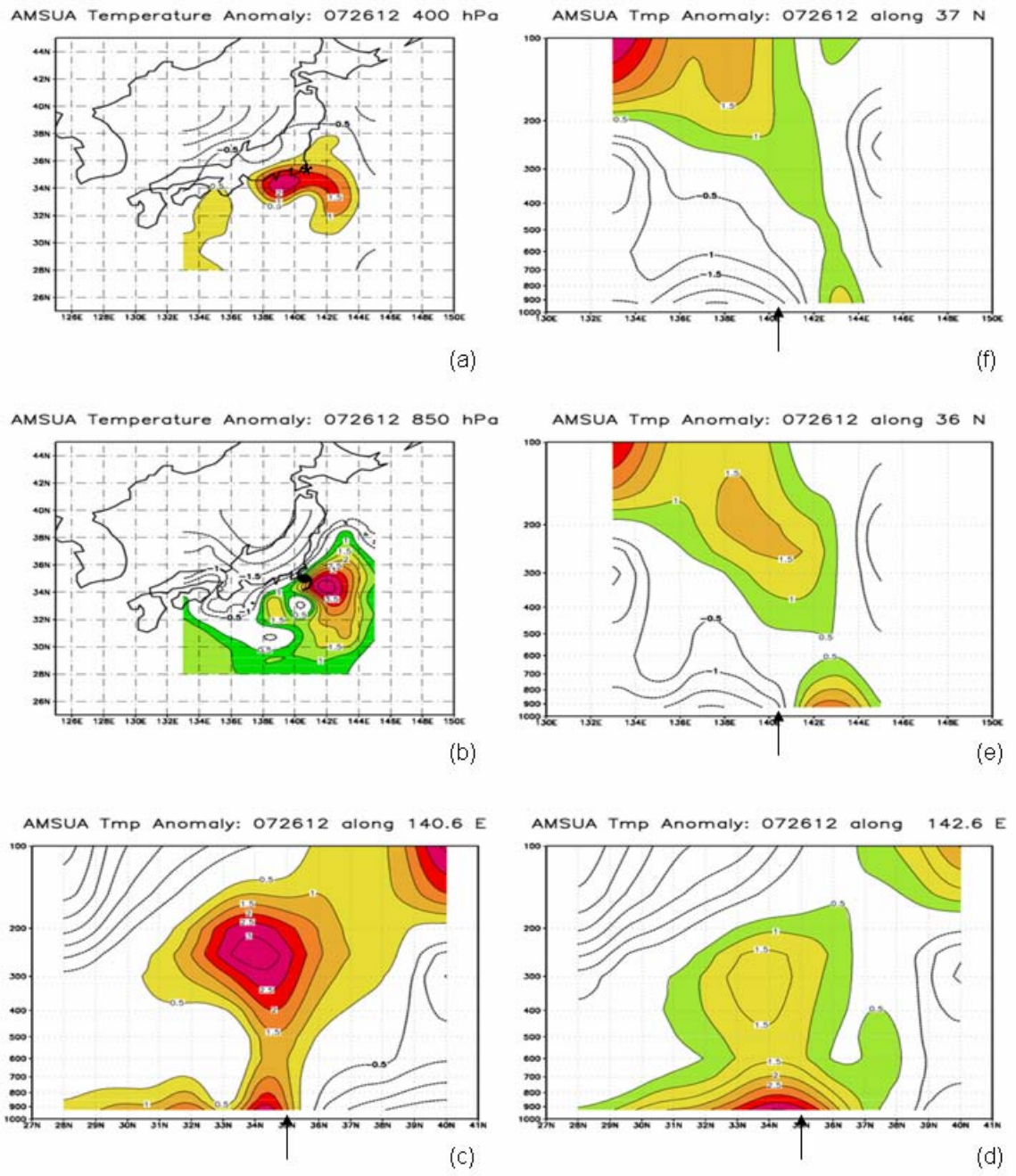

Figure 31. AMSU temperature anomaly at 1200 UTC 26 July (a) plan view, 400 hPa, (b) plan view, 850 hPa, (c) cross-section along 140.6° E, (d) cross-section along 142.6° E, (e) cross-section along 36° N, (f) Cross section along 37° N. The arrows along the abscissa indicates the position of the storm center.

C. POTENTIAL VORTICITY ANOMALY AND UPPER-LEVEL WIND STRUCTURE

Although the dynamic and thermodynamic processes discussed in the previous section contribute to the transformation of the tropical cyclone to an extratropical cyclone, they also influence the development of the down-stream anticyclone. As Banyan approaches the trough moving off the East Asian coast, the jet streak to the north has a zonal orientation with negative PV anomalies on the anticyclonic shear side of the jet streak (Figure 32). The anticyclonic curvature in the outflow of Banyan also is associated with a small negative PV anomaly (Figure 32). The trough approaching Banyan from the East Asian coast is evident as a region of positive PV anomaly.

At 0000 UTC 26 July (Figure 33), the outflow from Banyan has a larger anticyclonic curvature as the subtropical ridge builds northward in response to the thermodynamic forcing described in the previous section. The merger between the weak anticyclonic curvature of the jet streak and the strong anticyclonic curvature of the tropical outflow has begun. The areal extent of negative PV anomaly has increased to the east of the center of the decaying Banyan in response to the vertical motion and temperature distributions (Figure 26).

As Banyan begins the transformation stage at 1200 UTC 26 July (Figure 34), the jet streak and storm outflow have completely merged while maintaining a large anticyclonic curvature. At this time, the distribution of upward vertical motion is concentrated to the east of the storm center (Figure 27b) and corresponds to the large region of negative upper-level PV anomaly in Figure 34. The PV

anomaly east of the circulation of Banyan has become increasingly negative and has expanded over a larger area in association with an increase in the anticyclonic curvature. This process continues in a similar manner throughout the transformation stage (not shown).

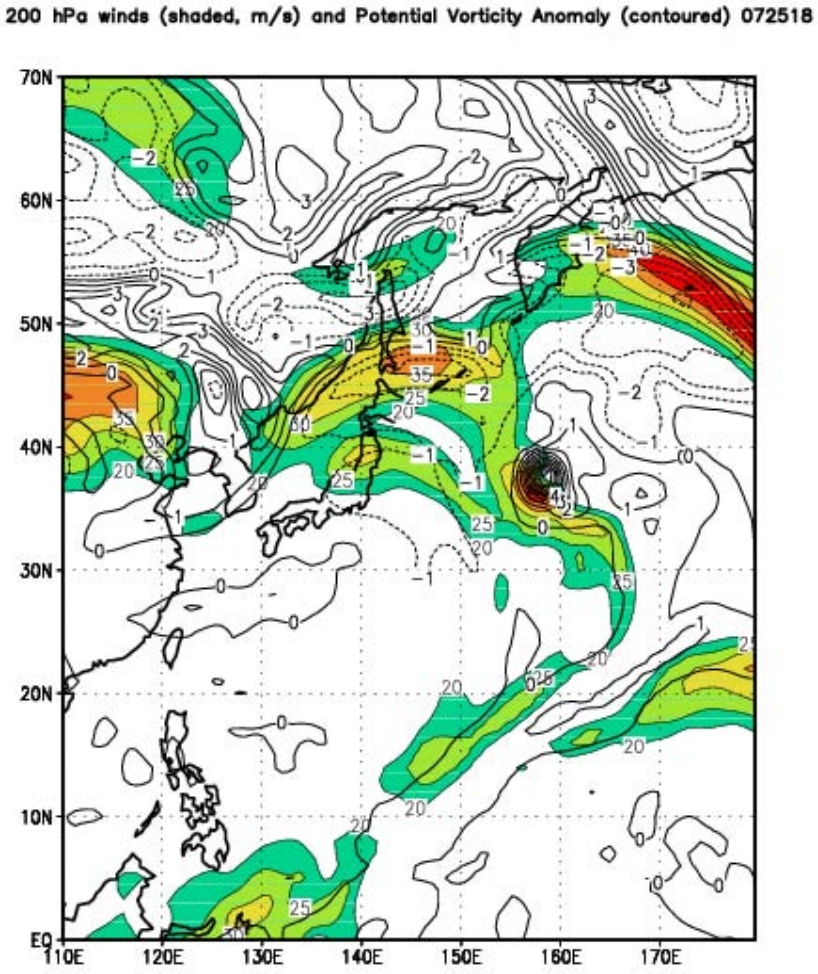

Figure 32. Isotachs at 200 hPa (shaded, 5 m s^{-1} interval) and potential vorticity anomaly at 200 hPa (contoured, 1 PVU) at 1800 UTC 25 July.

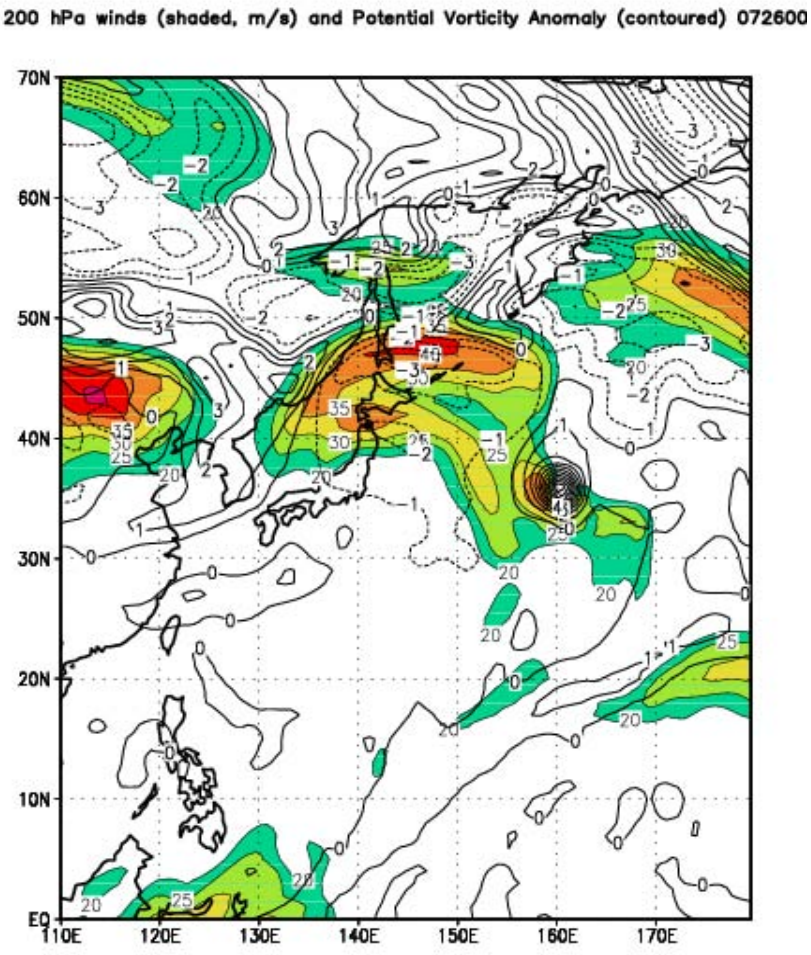

Figure 33. As in Figure 32, except for 0000 UTC 26 July.

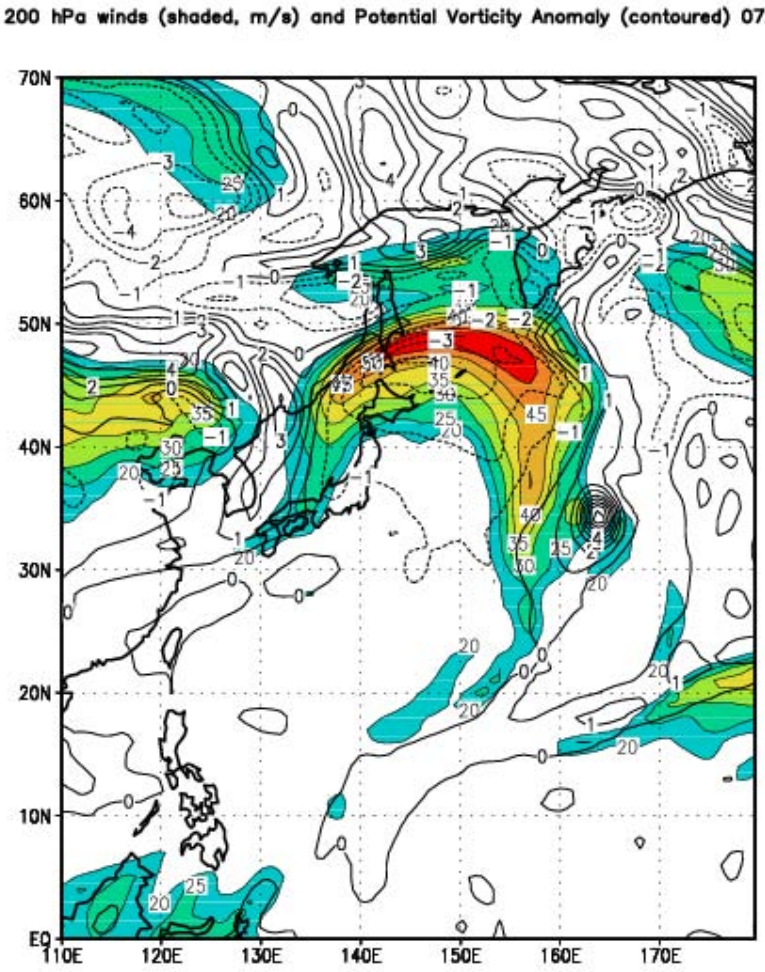

Figure 34. As in Figure 32, except for 1200 UTC 26 July.

Area averages were constructed and will be used to summarize the relationships between the upper-level wind pattern, upper-level PV anomaly distribution, and the distribution of midtropospheric vertical motion area averages were constructed. The 200 hPa wind speed (Figure 35) was averaged at each synoptic time from 1200 UTC 25 July until 0000 UTC 27 July in a 4 deg. lat. by 10 deg. long. region centered 8 deg. lat. north of the storm. The

selection of this region allowed the detection of the jet streak as the storm progressed northward. The vertical motion (omega) was averaged in the same manner in a box of the same dimensions, but centered 4 deg. lat. north of the storm (Figure 36). The PV anomaly (Figure 37) was averaged over a fixed region from 40°-50°N and from 140°-160°E, which was the region adjacent and east of the poleward track of Banyan.

As the upper-level wind speed increases, the upward vertical motion increases (omega becomes more negative), and both the fields reach their respective (absolute) maximum values at 1800 UTC 26 July. These two parameters are related to the upward vertical motion increasing in the right-entrance region of the jet streak as the outflow of Banyan merged with the midlatitude jet. The distributions of vertical motion and moist air suggest that the relationship between the jet and the thermodynamics north of the decaying tropical cyclone contribute to the northward and westward tilt of the midtroposphere warm anomaly (Figure 25). The negative PV anomaly steadily increases (in magnitude) beginning at 1200 UTC 25 July and reaches its most negative value (most anticyclonic) six hours after the 200 hPa winds and 500 hPa omega peak at 0000 UTC 27 July.

The dynamic and thermodynamic processes discussed in Chapter III.B. appear to be important precursors to the generation of the upper-level PV anomaly associated with the ET of TY Banyan. The dynamic and thermodynamic forcing in the middle- and lower-troposphere are noticeable in changes in the magnitude of the upper-level PV anomaly.

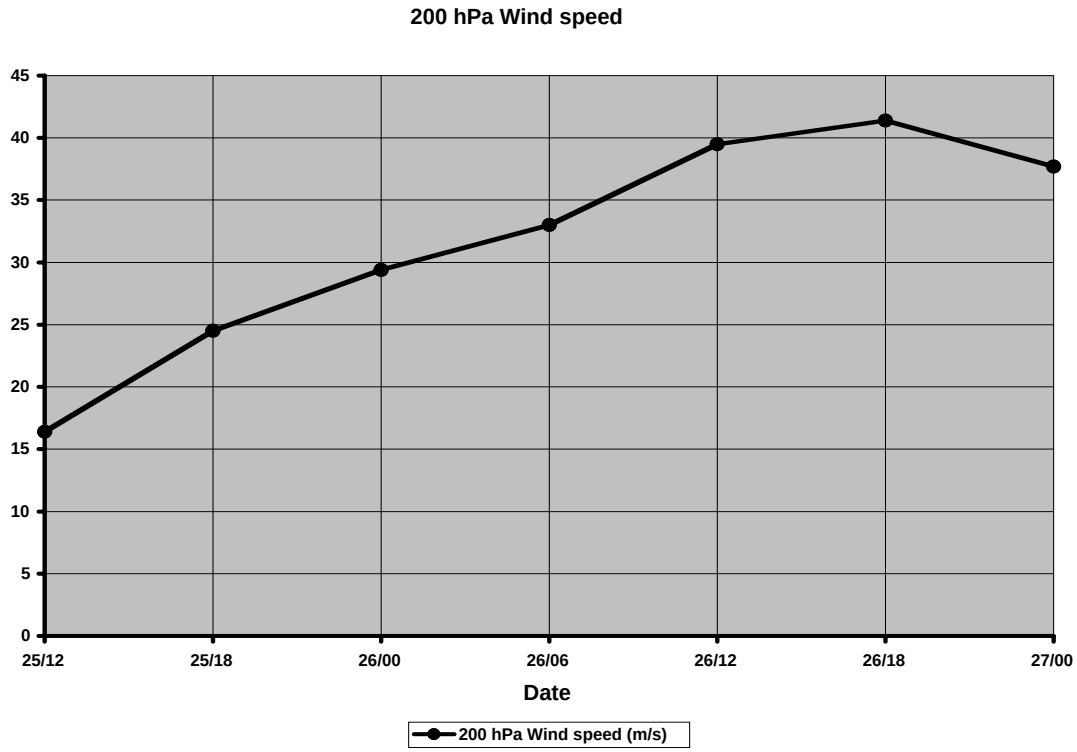

Figure 35. Average 200 hPa wind speeds (m s^{-1}) over the jet streak region by synoptic time.

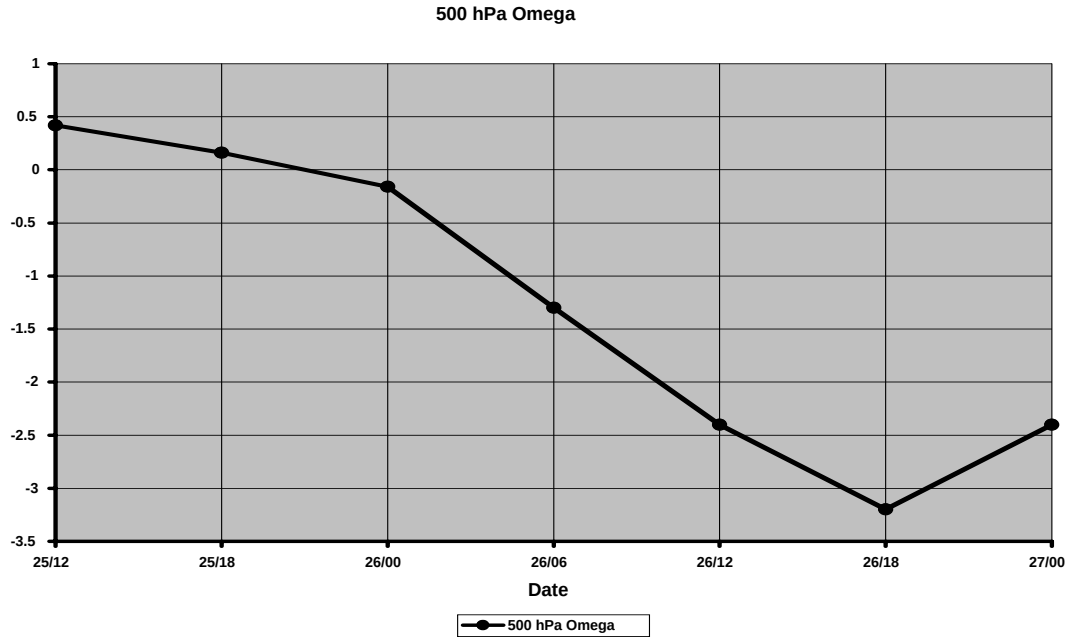

Figure 36. As in Figure 35, except for omega (μb s^{-1}) in a box 4° lat. to the north of the storm.

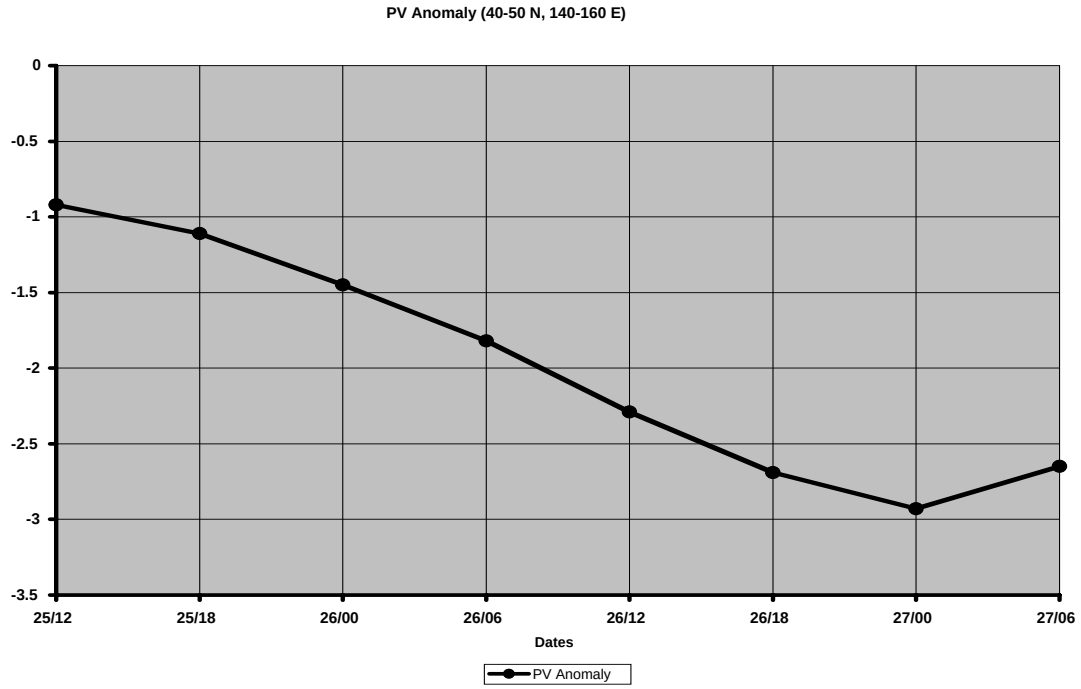

Figure 37. Average value of potential vorticity anomaly (PVU) in a region from 40°-50°N and 140°-160°E by date.

IV. SUMMARY AND RECOMMENDATIONS

A. SUMMARY

The process of ET is complex. During the transformation stage the tropical cyclone undergoes many changes under the influence of the baroclinic mid-latitude environment. This influence can be difficult to detect given the data sparse regions typical over which ET occurs. The use of satellite-based sensors in conjunction with model reanalyses greatly aids the researcher in understanding the processes involved in ET.

A schematic of the sequence of events described in this study is given in Figure 38. The sequence begins (Figure 38a) with an upright tower of positive PV associated with the mature tropical cyclone, with a region of upper-level negative $\frac{d\left(\overline{PV}\right)}{dt}$ that represents the TC outflow region. A region of upper-level positive potential vorticity associated with the midlatitude trough approaches the tropical cyclone from the west (Figure 38b), and this is preceded by a region of positive $\frac{d\left(\overline{PV}\right)}{dt}$ due to horizontal advection. The approach of this upper-level positive PV contributes to an asymmetry in the distribution of vertical motion and moisture around the tropical cyclone. This asymmetry results in an increase in upward vertical motion to the east of the storm. The warm advection and upward motion of moist air with the associated release of latent heat on the east side of the storm contributes to mid-tropospheric warming, which is associated with a positive

PV anomaly at low levels, and also contributes to the increased negative PV anomaly at the upper levels (Figure 38c). The low-level PV increase to the east of the tropical cyclone (Figure 38c) is due to a combination of positive PV advection around the decaying tropical cyclone and release of latent heat, which is evident in the cross section at 0000 UTC 27 July (Figure 29a). The upper-level negative $\frac{d\left(\overline{PV}\right)}{dt}$ region also continues to increase in magnitude and size. In the final stage (Figure 38d), the low-level PV distribution is dominated by the PV east of the decaying tropical cyclone. The mid-level PV distribution is maximum over the remnants of the tropical cyclone. At upper levels, the PV distribution is dominated by the midlatitude trough to the west. Similar arguments can be made for the evolution of the temperature structure as defined in Figure 31.

The asymmetric vertical motion and warm advection patterns initiated by the approach of an upper-level trough from the west cause increased warming in the middle troposphere. This diabatic warming in turn contributes an upper-level negative PV anomaly that is reflected as a building downstream of the anticyclonic circulation at upper levels. The large anticyclone may then have a pronounced impact on the downstream flow patterns that are evident in Figure 4.

In the case of TY Banyan, one important factor in building the downstream anticyclone is the presence of mid-troposphere cyclones to the east of Banyan. These cyclones and the associated jet maximum serve to anchor the outflow

from Banyan as the outflow merges with a mid-latitude jet streak to the north, which causes a strongly anticyclonic curvature to the resulting merged jet-TC outflow region. The thermodynamic processes at lower levels are initially enhanced by the jet maximum associated with the mid-tropospheric cyclone, and later serve to enhance the upper-level anticyclone and build the subtropical ridge northward.

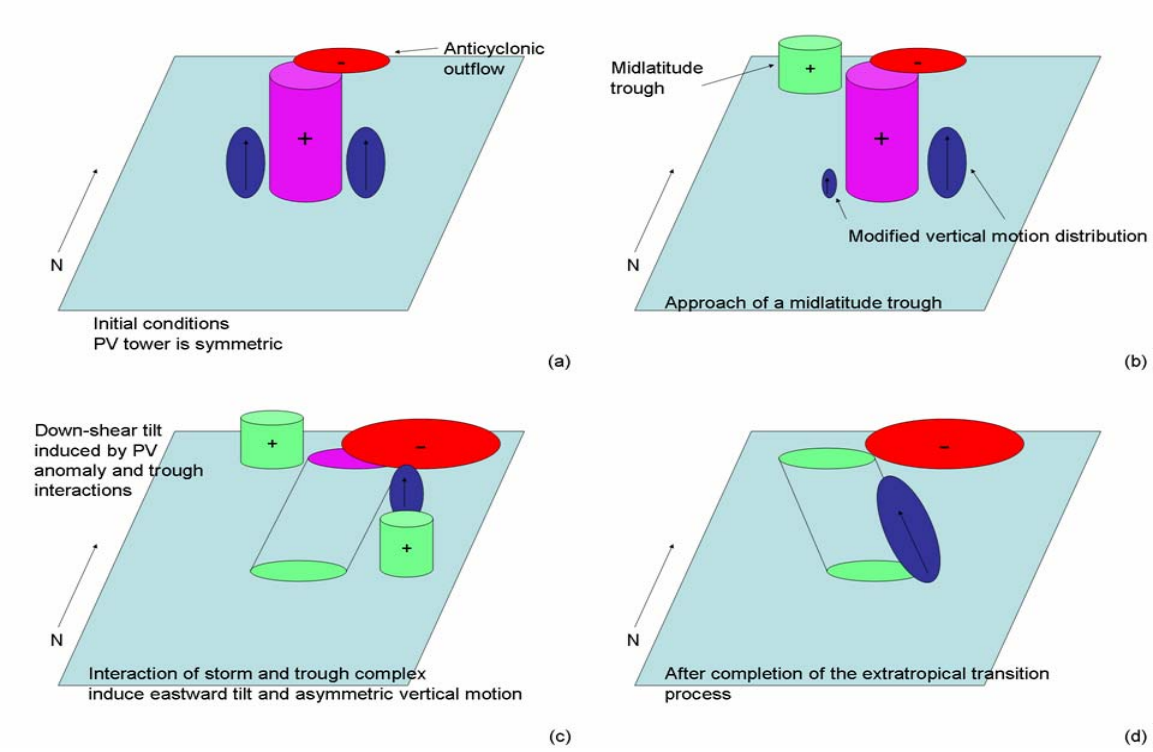

Figure 38. Generalized schematic showing the sequence of events for the ET of TY Banyan. Magenta indicates areas of positive potential vorticity anomaly associated with the TC, green indicates areas of positive potential vorticity anomaly associated with the midlatitudes and diabatic effects, red indicates areas of negative potential vorticity anomaly tendency at the upper levels, and blue regions of upward vertical motion and high relative humidity.

B. FUTURE RESEARCH OPPORTUNITIES

Many studies have addressed the transitioning tropical cyclone, as well as the resulting extratropical cyclone, but relatively few have addressed the building ridge caused by the strongly anticyclonic outflow from the decaying TC. Observational and modeling studies should be carried out to demonstrate the role of such a building ridge in the downstream impacts of ET.

To investigate the influence of the cyclonic circulation to the east of Banyan, a future research avenue could be to artificially remove this circulation from the model fields and re-run the models. This approach would allow determination of the role of this circulation in the ET of TY Banyan. Furthermore, it could aid in identifying the role of the anticyclone in influencing the downstream flow.

Another possible path of study is related to the robustness of the AMSU temperature anomaly patterns exhibited during the ET of TY Banyan. Do other storms completing ET have similar anomaly patterns? Can these anomaly patterns be determined objectively and in a timely enough manner to be of use to the forecaster? These questions will be difficult to answer until a more robust data set is developed.

LIST OF REFERENCES

Agusti-Panareda, A., C.D. Thorncroft, G.C. Craig, and S.L. Gray, 2004: The extratropical transition of hurricane Irene (1999): A potential-vorticity perspective. *Quart. J. Roy. Meteor. Soc.,* 130, 1047-1074.

Bessho, K., M. DeMaria, and J.A. Knaff, 2006: Tropical cyclone wind retrievals from the Advanced Microwave Sounding Unit: Application to surface wind analysis. *J. Appl. Meteor. Climatol.,* 45, 399-415.

Brand, S., and C.P. Guard, 1979: An observational study of extratropical storms that evolved from tropical cyclones in the western North Pacific. *J. Meteor. Soc. Japan,* 57, 479-482.

Cooperative Institute for Research in the Atmosphere AMSU website, cited 2006: Weighting function and data. [http://amsu.cira.colostate.edu/]

Demuth, J.L., M. DeMaria, and J.A. Knaff 2004: Evaluation of Advanced Microwave Sounding Unit tropical-cyclone intensity and size estimation algorithms. *J. of Appl. Meteor.*, 43, 282-296.

Demuth, J.L., M. DeMaria, and J.A. Knaff, 2005: Improvement of Advanced Microwave Sounding Unit tropical-cyclone intensity and size estimation algorithms. *J. of Appl. Meteor.,* submitted.

Digital Typhoon: Typhoon images and information, cited 2006: Digital Typhoon: single sequence view (Typhoon 200507/Banyan). [http://agora.ex.nii.ac.jp/digital-typhoon/summary/wnp/s/200507.html.en]

Goldberg, M.D., 2001: The limb adjustment of AMSU-A observations: Methodology and validation. *J. Appl. Meteor.,* 40, 70-83.

Goodrum, G., K.B. Kidwell, and W. Winston, (eds.), 2004: NOAA KLM user's guide. NOAA, NOAA-NESDIS/NCDC, Suitland, Maryland, USA.

Harr, P.A., and R.L. Elsberry, 2000: Extratropical transition of tropical cyclones over the western North Pacific. Part I: Evolution of structural characteristics during the transition process. *Mon. Wea. Rev.,* 128, 2613-2633.

Hart, R.E., and J.L. Evans, 2000: A climatology of the extratropical transition of Atlantic tropical cyclones. *J. Climate,* 14, 546-564.

Kidder, S. Q., M.D. Goldberg, R.M. Zehr, M. DeMaria, J.F.W. Purdom, C.S. Velden, N.C. Grody, and S.J. Kusselson, 2000: Satellite analysis of tropical cyclones using the Advanced Microwave Sounding Unit (AMSU). *Bull. Amer. Meteor. Soc.,* 81, 1241-1259.

Klein, P.M., P.A. Harr, and R.L. Elsberry, 2000: Extratropical transition of western north Pacific tropical cyclones: An overview and conceptual model of the transformation stage. *Wea. Forecasting,* 15, 373-395.

Knaff, J.A., S.A. Seseske, M. DeMaria, and J.L. Demuth, 2004: On the influences of vertical wind shear on symmetric tropical cyclone structure derived from AMSU. *Mon. Wea. Rev., 132*, 2503-2510.

Jones, S.C., P.A. Harr, J. Abraham, L.F. Bosart, P.J. Bowyer, J.L. Evans, D.E. Hanley, B.N. Hanstrum, R.E. Hart, F. LaLaurette, M.R. Sinclair, R.K. Smith, and C. Thorncroft, 2003: The extratropical transition of tropical cyclones: Forecast challenges, current understanding, and future directions. *Wea. Forecasting,* 18, 1052-1092.

Matano, H., and M. Sekioka, 1971a: On the synoptic structure of Typhoon Cora, 1969, as the compound system of tropical and extratropical cyclones. *J. Meteor. Soc. Japan,* 49, 282-295.

Mo, T., 1999: AMSU-A antenna pattern corrections. *IEE Trans. Geosci. Remote Sens.,* 37, 103-112.

Stubblefield, C.L., 2005: Microwave estimates of the extratropical transition process. M.S. Thesis, Dept. of Meteorology, Naval Postgraduate School, Monterey, CA, 87 pp. [NTIS]

Zhao, L., and F. Weng, 2002: Retrieval of ice cloud parameters using the Advanced Microwave Sounding Unit. *J. Appl. Meteor.,* 41, 384-395.

Zhu, T., D.L. Zhang, and F. Weng, 2002: Impact of the Advanced Microwave Sounding Unit measurements on hurricane prediction. *Mon. Wea. Rev.,* 130, 2416-2432.

THIS PAGE INTENTIONALLY LEFT BLANK

INITIAL DISTRIBUTION LIST

1. Defense Technical Information Center
   Ft. Belvoir, Virginia

2. Dudley Knox Library
   Naval Postgraduate School
   Monterey, California

3. Superintendent
   Naval Research Laboratory
   Monterey, California

4. Professor Patrick Harr
   Naval Postgraduate School
   Monterey, California

5. Professor Russell Elsberry
   Naval Postgraduate School
   Monterey, California

6. Professor Phil Durkee
   Naval Postgraduate School
   Monterey, California

7. Professor Carl Pfeiffer
   Naval Postgraduate School
   Monterey, California

8. Mr. Jeff Hawkins
   Naval Research Laboratory
   Monterey, California

9. Mr. Steve Tracton
   Office of Naval Research
   Arlington, Virginia

10. Dr. John Knaff
    Cooperative Institute for Research in the Atmosphere
    Boulder, Colorado

11. Director, Joint Typhoon Warning Center
    Naval Pacific Meteorology and Oceanography Center
    Pearl Harbor, Hawaii

12. Lieutenant Michael Vancas
Naval Pacific Meteorology and Oceanography Center
Pearl Harbor, Hawaii